Science of Remote Sensing 12 (2025) 100242

Contents lists available at ScienceDirect

Science of Remote Sensing

journal homepage: www.sciencedirect.com/journal/science-of-remote-sensing

Full length article

Accounting for seasonal retrieval errors in the merging of multi-sensor satellite soil moisture products

Pietro Stradiotti *, Alexander Gruber, Wolfgang Preimesberger, Wouter Dorigo

Department of Geodesy and Geoinformation, Technische Universitaet Wien, Wiedner Hauptstrasse 8–10, Vienna, 1040, Austria

ARTICLE INFO

Dataset link: https://doi.org/10.48436/z0zzp-f4j39

Keywords:
Soil moisture climate data record
Multi-satellite merging
Triple collocation analysis
Seasonal errors
Soil moisture uncertainty

ABSTRACT

ESA CCI soil moisture (SM) merges satellite microwave remote sensing datasets by means of their inverse-uncertainty weighted average. Estimates of uncertainty are produced with Triple Collocation Analysis (TCA) and assume a constant level of noise for the entire sensor period. However, errors in soil moisture retrievals vary throughout the year, since many impacting environmental parameters are characterized by a seasonality of their own. Here, we attempt to quantify this seasonal component and assess the impact of time-variant uncertainty estimates on the quality of merged soil moisture. We derive a long-term error variance estimate for three satellite products (from ASCAT, AMSR2, and SMAP) per day of year using a sliding window of 90 days. Merging weights climatologies are subsequently obtained as the inverse of such uncertainty. We analyse the impact of the modified approach by comparison with the merging based on stationary uncertainties/weights. The two key findings are that (i) the merged soil moisture estimates do not differ significantly between the stationary and the seasonal merging because seasonal uncertainty variations, e.g. caused by vegetation cover, usually affect all satellite missions in a similar way and thus cause only marginal changes in their relative weighting; yet, (ii) an evaluation against in situ data suggests that the estimated uncertainties of the new merged product are more representative of their seasonal behaviour. Based on these findings, we conclude that using a seasonal TCA approach can add value to merged products such as the ESA CCI SM by providing a more realistic characterization of dataset uncertainty – in particular its temporal variation.

1. Introduction

An integral part of Climate Data Records (CDRs) of any variable is the inclusion of well-described, self-consistent, physically justified, and validated uncertainty information (Merchant et al., 2017). Such information caters for a variety of applications, such as justifying the level of constraint of climate models with observations (Notz, 2015) or enabling model-data integration though assimilation (Reichle et al., 2008). A precise understanding of the spatio-temporal drivers of uncertainty is also fundamental in the process of data creation itself. For instance, the uncertainty of lower level (i.e., swath-format, single sensor) inputs should be accounted for when the data are aggregated into multisource gridded products. The European Space Agency's Climate Change Initiative for soil moisture (ESA CCI SM) is an example where multimission data is harmonized into a long-term record while accounting for uncertainties in the retrieval of each mission (Gruber et al., 2019; Dorigo et al., 2017). There, estimates of inverse-uncertainty weights are used by a weighted merging of distinct soil moisture time series to obtain a product with a comparatively lower observational uncertainty (Gruber et al., 2017). Nonetheless, weighted merging is only preferred over arithmetic averaging if the uncertainties – from which the weights are derived – can be estimated accurately (Reichle et al., 2008). In addition, to be instrumental, the uncertainties need to be consistent between products (that is, they should not reflect systematic biases between them), and should be complete in time and space (Gruber et al., 2017).

In the context of error-informed merging, uncertainty estimates that are sometimes provided with the individual sensor products (e.g., Parinussa et al., 2011; Naeimi et al., 2009) cannot be readily exploited since the propagation scheme is typically inconsistent between the various retrieval algorithms and observation principles (i.e., radiometric or scatterometric) of L2 data – all of which can lead to estimation biases. In addition, error propagation accounts for the sequence of retrieval transformations and the parameterization uncertainties, but not for the assumptions incorporated in the retrieval model itself (Merchant et al., 2017). As a result, the given uncertainty is underestimated when local conditions violate such assumptions. Alternatively, Triple Collocation Analysis (TCA) (Stoffelen, 1998) is an error diagnostic tool used prominently in the remote sensing of soil moisture (Scipal et al., 2008; Dorigo et al., 2010; Gruber et al., 2016). It aims to resolve

* Corresponding author.
E-mail address: pietro.stradiotti@geo.tuwien.ac.at (P. Stradiotti).

https://doi.org/10.1016/j.srs.2025.100242
Received 18 February 2025; Received in revised form 12 April 2025; Accepted 29 May 2025
Available online 11 July 2025

the random error variance (σ_ε^2) of three spatio-temporally collocated datasets with respect to the unknown truth that each observes using their temporal (co)variances. Unlike the error propagation approach, it is unaware of each exact transformations (and related error covariance matrix) in the retrieval chain, and implicitly includes failures of model assumptions, geo-location, or other unaccounted errors.

In order to obtain precise error variance estimates from TCA, a large enough number of collocated observations in the time series must be available, as otherwise the covariance matrix between the three time series is poorly defined and the error variance estimates unstable as a result (Zwieback et al., 2012b). For this reason, ESA CCI SM has so far used all available data points in the construction of the TCA triplet, which provides a single error variance estimate for a given location and sensor. In contrast to such stationary TCA approach, it has become evident that the uncertainty in satellite-based soil moisture varies at several temporal scales (Su et al., 2014), following dynamic conditions on the land surface which affect the sensitivity of the sensors to soil moisture (Loew and Schlenz, 2011; Wu et al., 2021). For example, the microwave signal attenuation from the vegetation layer – which is undisputedly one of the most prominent causes of uncertainties in soil moisture retrievals (Brocca et al., 2011) – follows seasonal phenological cycles that need to be corrected for in the retrieval (Vreugdenhil et al., 2016) or otherwise can lead to temporally-varying uncertainties in the retrieved soil moisture (Zwieback et al., 2018). Wu et al. (2021) provide an exhaustive description of such effect by analysing time-lagged correlation dynamics between (rainfall-driven) vegetation growth and TCA-derived soil moisture retrieval error. Moreover, backscatter signal inversions, which contradict the soil moisture-scattering linearity assumed by many retrieval models (Wagner et al., 1999; Owe et al., 2008), occur in the dry season due to subsurface scattering phenomena (Wagner et al., 2024) causing seasonal uncertainty variations which can deter the applicability of satellite soil moisture for drought monitoring applications (Vreugdenhil et al., 2022). Although not yet linked to subsurface scattering phenomena, the uncertainty in soil moisture derived from microwave brightness temperatures was also found higher in the dry-season (Loew and Schlenz, 2011).

The evidence of seasonal error sources has potential implications when these errors are quantified and adopted for the uncertainty-based merging of soil moisture. The first question we want to address here is whether the seasonalities of the input products uncertainties covary in time – leaving their relative weights unchanged, similar as in the stationary-uncertainty approach – or if instead they act complementarily, resulting in a change of the merged soil moisture compared to static merging. It should also be assessed whether the soil moisture error based on seasonally-dynamic merging is more representative of the actual soil moisture error than that resulting from a static merging. Answering these questions is not only relevant for the merging design of the ESA CCI SM dataset considered here, but also for other multi-sensor (soil moisture) products.

Previous work has demonstrated that the merging improves after considering the input products synergies in a time-variant manner, rather than stationarily (Kim et al., 2016). However, in this case the merging was performed by optimizing the empirically-determined correlation with modelled references, which contrasts our objective to obtain a fully observation-based merging. Hence, we rely on the unbiased error characterization TCA technique which brings about a different challenge, where less accurate uncertainty estimates (hence merging weights) may result from the smaller sample size corresponding to the seasonal subsets used in the dynamic approach (Loew and Schlenz, 2011). Based on this, the present study evaluates the benefit of seasonally-derived TCA uncertainty estimates in the ESA CCI SM merging. We aim to quantitatively assess their seasonal variations and relative magnitude, and their impact on the merged soil moisture and its overall uncertainty. We limit the analysis to three satellite-derived (active C-band, and passive C- and L-band) and one modelled soil moisture products used as observational inputs and TCA-supporting data, respectively. We further use uncertainty estimates derived from in situ data as a way to validate the uncertainty provided with the merged product.

2. Data

Soil moisture observations from the Advanced SCATterometer (ASCAT), the Advanced Microwave Scanning Radiometer 2 (AMSR2), and the Soil Moisture Active Passive (SMAP) missions can be complementary depending on the land surface and vegetation conditions, due to the different measurement technologies (passive/active) and microwave frequency (C-/L-band) employed (Kim et al., 2018). Here, we investigate how their synergies change in time and how they play out in the season-based merging approach.

The product specifics are detailed in Section 2.1 and summarized in Table 1. To form the TCA data triplets, soil moisture estimates from the Global Land Data Assimilation System (GLDAS) are used (Section 2.2). The in situ data selection for the method benchmarking is given in Section 2.3.

2.1. Satellite soil moisture

2.1.1. ASCAT

The active EUMETSAT H SAF ASCAT SSM product H120 (SAF, 2021) is derived from backscatter measured by the identical scatterometers onboard the satellite series Metop-A, -B and -C using the TU Wien soil moisture retrieval algorithm (TUW-SMR) at 12.5 km horizontal sampling (Wagner et al., 1999). ASCAT sensors measure microwave radiation in the C-band of the electromagnetic spectrum, where the backscatter has a pronounced sensitivity to soil moisture and a penetration depth of just a few cm into the topsoil (Wagner et al., 2013). At this frequency, structural vegetation elements attenuate the backscatter signal, making it challenging to resolve soil moisture in densely vegetated areas (Draper et al., 2013), despite the dedicated vegetation parameterization in the retrieval model (Vreugdenhil et al., 2016). In addition, soil moisture measurements from active microwave observations are deteriorated by surface roughness (Wagner et al., 2013) and dry soil conditions that may lead to subsurface scattering (Wagner et al., 2024).

A positive bias (i.e., wetter soil) in the observations from ASCAT-B was noticed with respect to ASCAT-C (and -A) on a global level (Scanlon et al., 2022), which may result in merged ASCAT time series with temporal breaks (Preimesberger et al., 2021) at the start of the ASCAT-C period. To account for this, we rescale the retrieved soil moisture signal from ASCAT-B to ASCAT-A by matching their distributions through linear scaling between distinct quantile bins, as described in Liu et al. (2011), Moesinger et al. (2020). Later, we merge ASCAT-A, -B, and -C via a simple average of the spatially and temporally collocated, overlapping observations. All sensors of the ASCAT series have identical instrument specifications and are assumed here to have homogeneous random error levels.

2.1.2. Passive products

Surface soil moisture from SMAP and AMSR2 is based on the Land Parameter Retrieval Model (LPRM (Owe et al., 2008; van der Schalie et al., 2017). LPRM allows for the simultaneous retrieval of Vegetation Optical Depth (VOD) and soil moisture in Ku, C, X and L-band (van der Schalie et al., 2017). The brightness temperature observations are acquired from the AMSR2 sensor onboard the GCOM-W1 satellite and from SMAP and resampled from the original resolution to a 0.25° grid. Given that AMSR2 measures in multiple bands, we give preference to C-band observations, and only use X-band observations to fill the gaps. SMAP acquires observations in L-Band, which achieves a better penetration of the vegetation layer, and is often considered optimal for soil moisture retrieval (Kerr et al., 2010). Although LPRM allows for day-time soil moisture retrievals, a decision is made to only use night-time observations due to the comparatively better quality w.r.t. the instable diurnal retrievals (Parinussa et al.), for both sensors. We mask the soil moisture with the LPRM quality flags raised in case of frozen soil or barren ground (van der Vliet et al., 2020), dense vegetation or potential radio frequency interference (RFI) contamination for specific

Table 1
Specifics of the satellite products used in this study.

	ASCAT	AMSR2	SMAP
Product source	EUMETSAT H SAF	JAXA G-Portal	NASA EarthData
Platform	METOP-A/B/C	GCOM-W1	SMAP
Product (Producer)	H120 (EUMETSAT H SAF)	LPRM (Planet)	LPRM (Planet)
Product algorithm (version)	TUW-SMR (v7)	LPRM (v7.0)	LPRM (v6.2)
Overpass local time	09:30/21.30 (Desc./Asc.)	01:30 (Desc.)	06:00 (Desc.)
Period used	Sep 2012-Dec 2023	May 2012-Dec 2023	April 2015-Dec 2023
Revisit time (days)	~1	~2	~2-3
Channel (freq. band) used	5.3 GHz (C)	6.925/7.3/10.65 GHz (C1/C2/X)	1.4 GHz (L)
Original horizontal resolution (km)	25	46	43
Retrieval Unit of soil moisture	Degree of saturation (%)	Volumetric ($m^3 * m^{-3}$)	Volumetric ($m^3 * m^{-3}$)

locations (de Nijs et al., 2015). Errors in passive soil moisture originate from the water contained in vegetation (as discussed for active systems) and from errors in the supporting data (e.g., skin temperature or soil composition), as well as approximations in the retrieval model design (Parinussa et al., 2011).

VOD is a model parameter that is derived along with soil moisture by LPRM. It quantifies the volume scattering and signal attenuation effects of the vegetation covering the soil, which has been previously used – as is used here – as a proxy of the soil moisture uncertainty (Gruber et al., 2016). For this study, VOD data is obtained from the LPRM retrieval of AMSR2 in C-band and masked as described above for soil moisture. While the dense vegetation masking is not necessary in this case, VOD is effectively only used where soil moisture observations are available.

2.1.3. Data collocation and masking

To collocate the datasets in space, ASCAT needs to be first resampled to the same 0.25° regular grid shared by ESA CCI SM, LPRM, and the model (Section 2.2). For this, a moving Hamming window with a search radius of 25 km and a minimum number of three neighbours is used. Only valid data points are included in the resampling since (similarly to LPRM) flags are raised in case of frozen ground, retrieval failure (i.e., out-of-bound soil moisture values), and additionally in case of volume scattering from sand. For all products, only time information on the respective acquisition day is retained, as the merged product is formally provided at daily resolution. A further collocation with the model for the TCA is described in Section 3.2. The masking of freezing/thaw is complemented by simultaneous use of information from the ASCAT and LPRM products, with the goal of homogenizing this key data quality aspect (van der Vliet et al., 2020). Therefore, days where at least one of the satellite datasets indicates frozen ground conditions are masked in all datasets, while the model is masked separately.

2.2. Model product

The Land Surface Model (LSM) Global Land Data Assimilation System (GLDAS) (Rodell et al., 2004) Noah L4, v2.1 is chosen to provide a third TCA dataset and an internally consistent climatology reference of more than two decades to which the satellite data is rescaled. GLDAS-Noah v2.1 provides 3-hourly estimates of soil moisture at several depth layers at 0.25° resolution, of which a daily average of the uppermost layer (0–10 cm) only is used. The model estimates are masked if the temperature variable from the same layer is below 0 °C.

2.3. In situ reference

The International Soil Moisture Network (ISMN) centralizes the collection of soil moisture data from regional in situ networks on a global scale (Dorigo et al., 2021). Here, all sensors measuring soil moisture in the period 2015–2023 at a depth between 0–10 cm are considered (Fig. A.11, Table A.2). After removal of all data points not marked as "good" ("G" flag) (Dorigo et al., 2013), the originally hourly observations within a day are averaged to match the temporal resolution of the satellite products.

2.4. ESA CCI landcover

Coarse vegetation classifications can be used to discriminate between different absolute levels of soil moisture errors (Wu et al., 2021), helping to separately assess their impact on the merging. Here, the results are stratified based on the landcover data of ESA CCI v2.0.7 (E.S.A. Land Cover C.C.I. project team and Defourny, 2019) for the year 2015. We employed the CCI-landcover User Tool to aggregate the original 300 m horizontal resolution values to the 0.25° grid used here, and further selected only locations with a majority land cover class abundance higher than 40% at the quarter-degree level to avoid mixed-pixel results. The original classes were then grouped thematically according to Table A.3 (Fig. 3b), leading to a clear-cut separation of vegetation regimes (Fig. A.12).

3. Methods

In this study, we employ an adaptation of the current ESA CCI SM merging approach, which focuses on the uncertainty characterization and consequent weight estimation for the merging. This is only one aspect of the full merging algorithm, which comprises, sequentially: removal of the inter-sensor biases, characterization of their uncertainties, uncertainty gap-filling, weights-based merging (Gruber et al., 2019), and break homogenization (Preimesberger et al., 2021). For context, we briefly review the merging algorithm as described in the latest product documentation (Dorigo et al., 2023) in Section 3.1 and afterwards focus on the innovation introduced in this study with respect to the ESA CCI SM baseline (Section 3.2).

3.1. Merging principle

Merging the input datasets into a single product θ_m requires finding the optimal weight parameters w to average the soil moisture inputs θ_i of the n considered sensors (which vary per location and day):

$$\theta_m = f(\theta_1, \ldots, \theta_n) = \sum_{i=1}^{n} w_i \theta_i \tag{1}$$

with associated soil moisture error variance σ^2_ϵ of the merged product resulting from analytical uncertainty propagation of the merging equation:

$$\sigma^2_{\epsilon,m} = \sum_{i=1}^{N} \left(\frac{\partial f(\theta)}{\partial \theta_i} \right)^2 \sigma^2_{\epsilon,i} = \sum_{i=1}^{N} w_i^2 \sigma^2_{\epsilon,i} \tag{2}$$

The weight associated to an input soil moisture observation is based on the reciprocal of its estimated random error, meaning that the measurements with a lower random error are weighted higher for merging:

$$w_i = \frac{1/\sigma^2_{\epsilon,i}}{\sum_{n=1}^{N} 1/\sigma^2_{\epsilon,n}} \tag{3}$$

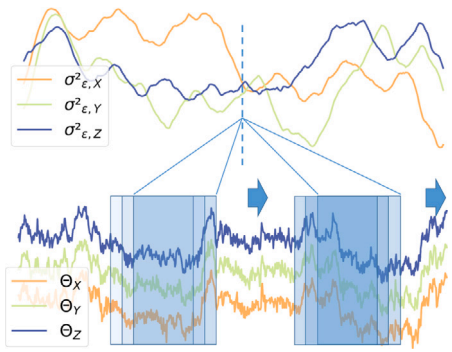

Fig. 1. Schematic of the sliding window for the uncertainty estimation over the three input timeseries.

The uncertainty itself is computed with TCA. Provided a set of three time series X, Y, Z, the random error variance of each can be resolved by a system of three equations of the form (here for X):

$$\sigma^2_{\epsilon_X} = \sigma^2_X - \frac{\sigma_{XY}\sigma_{XZ}}{\sigma_{YZ}} \tag{4}$$

where σ^2_X is the soil moisture signal variance and σ_{XY}, σ_{XZ}, and σ_{YZ} are the covariances between X and Y, X and Z, and Y and Z, respectively. Provided that all the assumptions (Gruber et al., 2016; Zwieback et al., 2012b) are met, this method provides an estimate of the error variance σ^2_ϵ of each dataset. However, this assumes that the derived uncertainties remain constant over time, while instead error sources may be characterized by their own climatology. Therefore, while the σ^2_ϵ value derived with this approach is representative of the average uncertainty, it fails to consider the potential presence of seasonalities therein.

3.2. Seasonal adaptation of TCA

In this study, we use the two TCA triplets $TCA_{SMAP-ASCAT-GLDAS}$ and $TCA_{AMSR2-ASCAT-GLDAS}$ to estimate the uncertainties of SMAP, and for AMSR2 and ASCAT, respectively. The latter triplet is used to provide the estimate for ASCAT since it counts more observations due to the longer AMSR2 record and higher revisit frequency compared to SMAP.

The system of linear equations based on Eq. (4) is then solved separately for each day-of-year (DOY) considering all available years, effectively obtaining a 366 data points climatology of the uncertainty estimates. This is achieved by sliding a multi-year window of 90 days centred around each DOY which wraps around the edges of each year (Fig. 1).

The intention here is to robustly characterize the vegetation-driven error and other components with seasonal repeat cycle. A window size of 90 days (which exceeds the 60 days window previously recommended by Kim et al., 2016) results in large global samples, although areas with annual freezing or snow cover only allow for uncertainty estimation for parts of the year (Fig. A.13). Similarly, no uncertainty estimates are provided for desert areas due to permanent barren ground flagging.

Note that the bias between the triplets is removed in the same temporally dynamic fashion, i.e., by performing the piecewise cumulative distribution function (CDF) matching of Liu et al. (2011) to 90-days, multi-year subsets of the entire time series. Using the same design as for the error estimation avoids incurring calibration errors that can lead to outliers or phase differences in the estimates (Zwieback et al., 2012a).

3.2.1. Masking of the uncertainty estimates

We mask the TCA-based estimates using a stationary p-value decision tree computed for a specific sensor combination and merging period based on the mutual correlations between datasets (Gruber et al., 2016), which helps determining whether the same phenomenon is observed by all datasets. Contrary to the TCA estimate itself, we do not evaluate the significance per DOY. This avoids observation-scarce periods (i.e., in winter time) to more often incur insignificant correlations due to the reduced sample size. Given that an unweighted average is used in such scenario, this would in turn lead to a systematic difference in the merging performance between observation-dense and observation-scarce periods. A stationary significance test is judged robust enough and yet indicative of the overall time series quality.

3.2.2. Uncertainties gap-filling

When the uncertainty estimates are missing, either because of the described masking or unstable TCA estimates, the strong general relationship between soil moisture errors and VOD can be used to fill these gaps in the uncertainty estimates (Gruber et al., 2016). We adapt this method to take into account seasonally-varying vegetation conditions, for improved interpolation of seasonal uncertainty estimates:

$$\sigma_{\epsilon,DOY} = \alpha + \beta_1 VOD^1_{DOY} + \cdots + \beta_n VOD^n_{DOY} \tag{5}$$

where α and β are the offset and polynomial coefficients, respectively, and n is the polynomial order which was determined empirically to obtain the best fit (Gruber et al., 2016). While Eq. (5) is also valid in case of stationary uncertainty and VOD estimates (i.e., one per time series), the seasonal estimates (as argued here) better represent both quantities and may thus improve the description of Eq. (5). Following this logic, all DOY σ^2_ϵ values are mapped to the corresponding DOY average VOD value from the AMSR2 (2012–2023) climatology, and used in the same regression pool. We also weight the regression points proportionally to $1/\sqrt{N}$ with N the number of data points used to derive the uncertainty estimates. This accounts for the impact of sample size on the accuracy of the TCA estimates. The so-derived coefficients are then used to gap-fill the uncertainty estimates from the VOD climatology in a temporally-dynamic manner.

3.3. Uncertainty evaluation

To provide a validation reference for the estimated soil moisture uncertainty, we first remove both additive and multiplicative biases between each in situ (θ_i) and merged (θ_m) satellite soil moisture observation series by matching their mean and standard deviation. Later, we evaluate the unbiased-Root Mean Squared Difference ($ubRMSD$) between θ_i and the bias-corrected product (θ'_m):

$$ubRMSD_{m,i} = \sqrt{\sum^{N} \frac{(\theta'_m - \theta_i)^2}{N}} \tag{6}$$

and compare it to the stationary and dynamically merged soil moisture uncertainty. For the computation of Eq. (6), a satellite-in situ data pair is only considered when the two are spatially collocated within 0.25° and within the same day. We further only consider the period of complete sensor availability (ASCAT, AMSR2, and SMAP) May 2015 - December 2023 to remove the effect of the sensor transitions, and disregard collocated time series that contain less than 25% of the possible observations.

4. Results and discussion

4.1. Climatological uncertainty estimates

We first evaluate the intra-annual variability in the uncertainty estimates of the input products by looking at the inter-quartile range (IQR) of their distribution (Fig. 2). The IQR is for all products in the

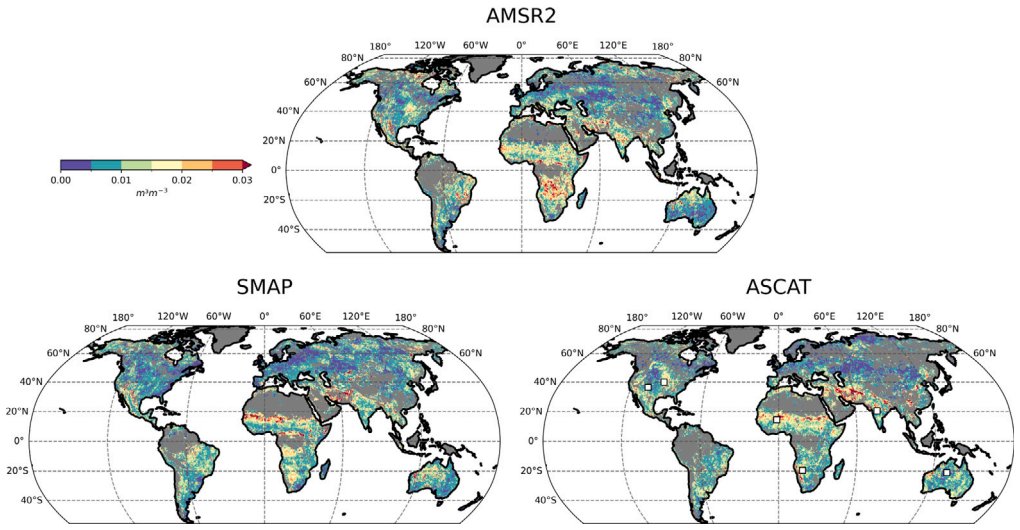

Fig. 2. IQR of the soil moisture uncertainty climatology for the input products before uncertainty/VOD regression gap-filling. Gaps are due to too few collocated data and *p-value* masking, and because the IQR is not shown if less than 30% of the 366 DOY values are available (to be compared with Fig. A.13 for reference). The points indicate the locations shown in Fig. 3.

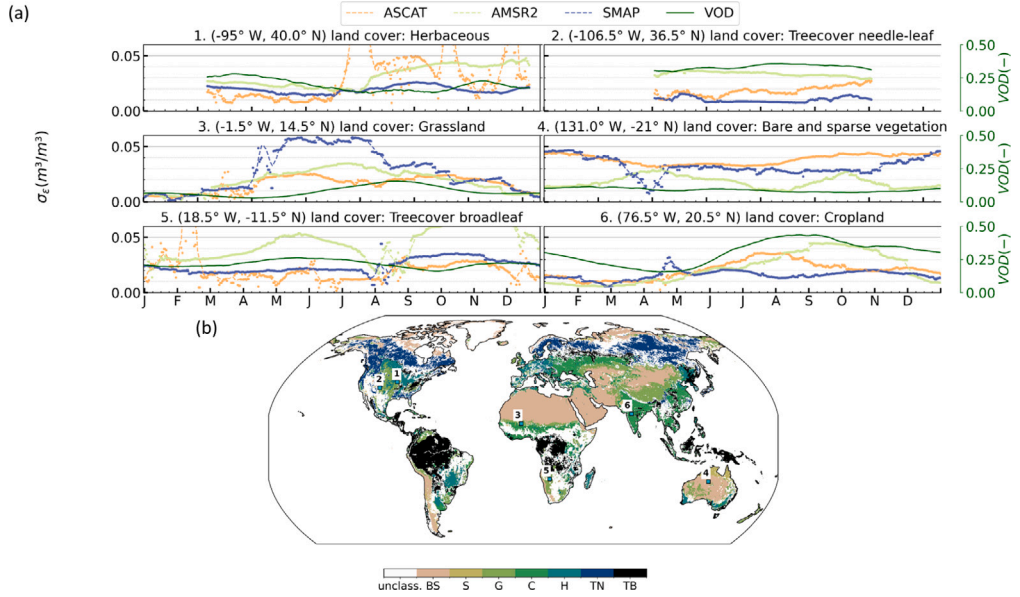

Fig. 3. (a) Input products uncertainty climatologies (before uncertainty/VOD regression gap-filling) and AMSR2 C-band VOD climatologies for the points shown in the (b) landcover aggregation map. Based on aggregated ESA CCI Landcover classes described in Table A.3.

$0.005 - 0.02 \quad m^3 * m^{-3}$ range, with the exception of a few outstanding regions where the spread exceeds the $0.03 \quad m^3 \quad * \quad m^{-3}$ value. For AMSR2, such high error variability regions are located at the edges of the densely forested regions of Eastern Brazil and south of Central Africa, in the grasslands and croplands of central India, and partly in the central US region between the eastern temperate forests and the Great Plains. With the exception of the latter region, the patterns are distinctly different for ASCAT, with a high range of uncertainty over the Sahel. High(er) variability is also observed in large parts of the Persian plateau, Australia, and Namibia. SMAP is generally more consistent with ASCAT than AMSR2, with the exception of Australia, where the variability patterns are roughly inverted.

Fig. 3a shows a direct comparison of the error climatologies with VOD for 6 arbitrary locations, hinting that fluctuations are not always explained by vegetation changes. For instance, at (1) the error of ASCAT increases sharply and becomes unstable in the second half of the year while no particular VOD changes are observed. Such oscillations of ASCAT in barren and low vegetation cover regions coincide well with subsurface scattering patterns (Wagner et al., 2024). In a similar way, the error in SMAP at (3) is suddenly driven up just before and during the Sahel wet season (JJA) but no changes of the same magnitude are observed for ASCAT and AMSR2. Similar but less extreme behaviours are present at (2) and (4), where observed uncertainty changes are not matched by similar variations in VOD. In contrast, at (5) and (6) the VOD behaves more coherently with the estimated soil moisture uncertainty and seems to explain well the observed fluctuations. Still, while the uncertainties are consistent in magnitude between the sensors at (6), the maximum uncertainty of SMAP and ASCAT is lower compared to that of AMSR2 at (5), reflecting the difficulty of passive C-band systems to resolve soil moisture under dense vegetation (Kim et al., 2018).

Note that the TCA estimates shown in Fig. 3a are derived from smaller samples (determined by the 90-days sliding window size) than are the static TCA estimates that are derived from the entire time series.

Hence, they are themselves subject to greater sampling uncertainty, which incurs in a more "noisy" appearance. The effective number of samples that is included in each DOY window varies by season and location (due to masking), and between the two triplet combinations (Fig. A.13). Nevertheless, with the current sliding window definition, the sample size after collocation is generally well above the often-recommended $N = 100$ value (corresponding to a $\sim 20\%$ of uncertainty on the error estimates (Zwieback et al., 2012b)), especially in the Southern Hemisphere (SH). At latitudes above $\sim 40°N$ the seasonal frozen soil/snow masking strongly affects the TCA sample size and causes it to vary throughout the year, while in the Arabic peninsula, Persian plateau, and in the Sahara desert regions observations are sparse due to barren ground masking. The less frequent revisit of SMAP (also visible for AMSR2 and ASCAT nearing the equator) decreases the observational density in the $TCA_{SMAP-ASCAT-GLDAS}$ triplet compared to $TCA_{AMSR2-ASCAT-GLDAS}$. Therefore, especially for the latter TCA combination, it is legitimate to question whether the increase in temporal information sought here justifies the heightened uncertainty in the σ_ϵ and weights estimates. This question boils down to a comparison between the uncertainty in the estimates (σ_σ, driven by the sample size) and the difference between a static all-year estimate and that provided by each temporal subset, σ_{DOY_i}. This trade-off might call for a sample-size conservative strategy at high latitudes where TCA estimates are more susceptible to errors (Dorigo et al., 2010), or favour the seasonal approach in the regions where a strong climatology of σ_ϵ is highlighted (Fig. 2). While the applied masking (Section 3.2.1) will partially mitigate the former case, a more meticulous approach in the merging algorithm could prove beneficial. Recent efforts have been undertaken to obtain such decision boundary based on bootstrapped confidence intervals of σ_ϵ (Formanek et al., 2025), and should be considered as a subsequent refinement of the algorithm. Here, we try to establish the merit of the seasonal adaptation prior to σ_σ considerations that similarly apply to the static merging scenario. In the present case, even considering only regions where the sampling-related uncertainty variability is at the lowest, strong error variability differences between the sensors are still observable, suggesting that the adapted TCA incorporates sensor-specific local differences. From the merging perspective of ESA CCI SM, such regions where sensors are singled out in terms of their intra-seasonal error fluctuations offer an opportunity to fine-tune the merging weights.

Notably, when calculating the annual mean of the climatological uncertainties, these means are typically smaller than the stationary uncertainty estimates that were generated from the entire time series directly. This is the case for all sensors (as visible from Fig. A.14). ASCAT shows the largest difference, which is consistent with previous studies (Wu et al., 2021). Nevertheless, our primary concern is not the absolute uncertainty estimates of the products, but rather their relative magnitude – which determines the consequent change in merging weights. However, it should be noticed that (i) the described bias is larger for ASCAT compared to AMSR2 and SMAP and (ii) due to such bias in all sensors, the merged uncertainty will be lower overall.

4.2. Relationship between uncertainties and impact on the merging weights

The Pearson correlation coefficients (R) of the σ_ϵ^2 climatologies shows that the best agreement globally is observed between the two passive sensors (Fig. 4). In contrast, active (ASCAT) shows several regions of null- or anticorrelation with AMSR2 (despite an overall good agreement) and SMAP, where null and weak anticorrelations are dominant outside of few local exceptions. The decorrelation of the SMAP and ASCAT uncertainties may be due to their specific sensitivity to vegetation change, as shown by the different response temporal lags to rainfall and vegetation (Wu et al., 2021). The correlation results suggest that the seasonal drivers of uncertainty are shared predominantly between sensors based on the same (active, passive) instrument type and retrieval model, and to a lesser extent between different microwave frequencies, confirming what seen on a time-stationary basis (Van der Schalie et al., 2018). As a result, merging synergies on a seasonal basis are to be looked mainly between active and passive sensors, confirming what previously found from a stationary perspective (Gruber et al., 2017).

A seasonality in the uncertainty of the individual sensors does not directly generate a seasonality of the merging weights, since temporally coherent variations between the sensors may leave Eq. (3) unchanged. Based on both seasonal variability and temporal coherence of the uncertainties, three merging weight scenarios can be outlined. In the first scenario, all the sensors have a similar seasonality, leaving the merging weights unchanged with respect to the stationary merging. This will reflect in seasonal effects of the merged soil moisture uncertainty, but not in a change of the muti-source soil moisture signal itself. This is the case, e.g., in the Sahel region and parts of the Indian subcontinent. In the second scenario, the seasonal merging can better make use of the intra-annual synergies between the sensors, corresponding to regions of lower uncertainty correlations between sensors in Fig. 4. In this case, the weights that are calculated from uncertainties with differing temporal fluctuations (Eq. (3)) will also exhibit a seasonal behaviour, and thus cause intra-annual changes in the merged soil moisture estimates as well.

In the absence of strong uncertainty oscillations, the σ_ϵ^2 climatologies generally correlate well. In this third case, we can expect that neither the merged soil moisture estimate nor its uncertainty will be significantly affected by the seasonal approach. This can be observed for instance in the western part of the Great Plains in North America and parts of South America.

The impact of the different scenarios on the merging weights can be assessed directly by looking at their aggregates over the ESA CCI-land cover classes (Fig. 5). The Southern Hemisphere (SH) alone is considered to avoid the SH-NH climatologies cancelling off, and since the impact of seasonally frozen soil masking is minimal here. The lancover types well distinguish between different merging weights regimes. On average, ASCAT is assigned a higher weight with increasing vegetation density, which is consistent with the stationary merging (Gruber et al., 2017). Except for the lowest vegetated class BS, SMAP is always preferred over AMSR2, and the climatological fluctuations are similar between the two. As a consequence, the main weights trade-off during the year occurs between active and passive sensors. The strongest weight variations are observed for the shrubland, cropland, herbacous, and grassland land cover types. ASCAT weights peak at the end of the SH Summer (February–March) in shrublands, but slightly later for croplands (May), and herbaceus cover (May–June).

Overall, the seasonal weights do not depart substantially from the static case for most land cover types. Where they do, the difference is confined to only parts of the year. This is consistent with the lack of strong anticorrelation in the uncertainty climatologies (Fig. 4), which implies that the seasonal errors affect the inputs in a similar way, and consequently lead to similar relative sensors weights for each DOY as in the stationary case. The ranking of sensors by weight is similarly consistent with the stationary case, except for the shrubland case, where the relative weighting of ASCAT and AMSR2 is roughly inverted.

4.3. Merged soil moisture comparison

Using the seasonal uncertainty estimates from Section 4.2, we assess the difference on the merged soil moisture (combining ASCAT, SMAP, and AMSR2) compared to the stationary merging approach by their $RMSD_\Theta$ (Fig. 6). We subset by season based on the expectation to see a different impact of the merging (e.g., the peak in the weight of ASCAT for the herbaceous cover only occurs in the SH Autumn and Winter, Fig. 5). The shrubland cover shows a clear lag between seasons in terms of $RMSD$, with the SH Summer showing the largest discrepancy between the two merged products. This is consistent with the fact that the intra-annual vegetation dynamics (in terms of VOD) for this landcover

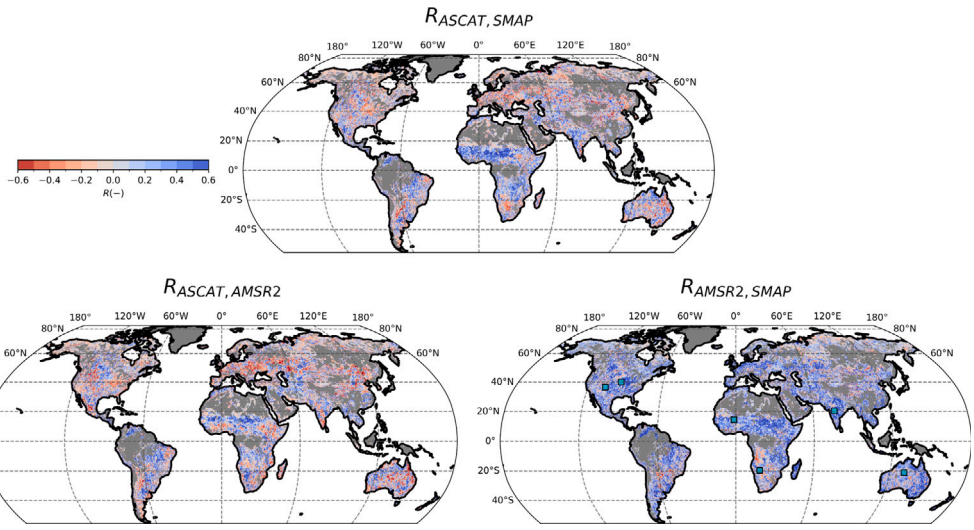

Fig. 4. Pearson R between the computed σ_ϵ^2 climatologies of the three sensors (before uncertainty/VOD regression gap-filling). Gaps are due to too few collocated data. The points indicate the locations shown in Fig. 3.

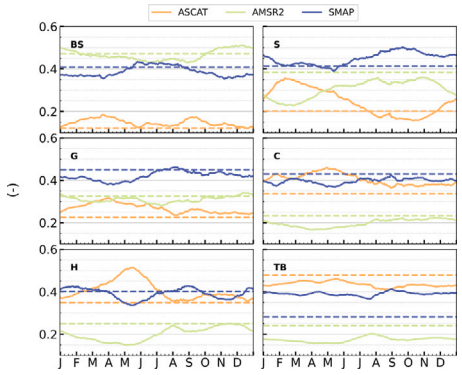

Fig. 5. Fractional weight applied to each sensor in the merging by landcover class. Each point represents the spatial median (SH only) for a certain DOY. The stationary weights are shown in the dashed line. Based on aggregated ESA CCI Landcover classes (BS: Bare and sparse vegetation, S: Shrubland, G: Grassland, C: Cropland, H: Herbaceous, TB: Treecover broadleaf, TN: Treecover needle-leaf) as described in Table A.3. The lancover classes are arranged by increasing mean VOD (Fig. A.12) from left to right, and from top to bottom.

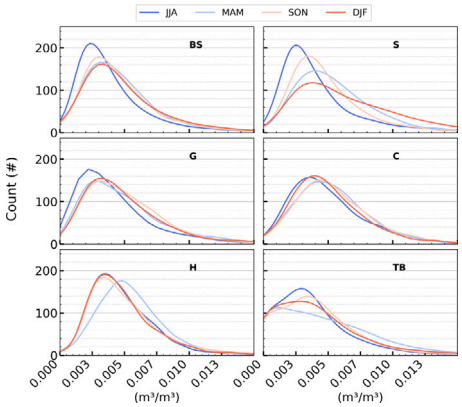

Fig. 6. Distribution of the $RMSD$ between the seasonally- and stationary-merged soil moisture products, by season and aggregated ESA CCI-land cover (SH only): BS: Bare and sparse vegetation, S: Shrubland, G: Grassland, C: Cropland, H: Herbaceous, TB: Tree cover broadleaf, TN: Tree cover needle-leaf) as described in Table A.3.

are very strong in the SH (Fig. A.12). Vegetation types with strong climatologies, like croplands and herbaceous covers, do not show as strong a separation. For the herbaceous cover, the separation is only visible between the SH Autumn (MAM) and the rest of the year. For croplands (and tree covers), the seasonal separation is not as evident. Despite the overall stationary vegetation regimes, barren ground/sparse vegetation and grasslands display a higher $RMSD$ during the year compared to the SH Winter. In this case, the difference is likely driven by other seasonal error sources than vegetation – subsurface scattering likely also not being the cause, given that a larger impact should be expected in the dry season (JJA).

The impact of the new merging on soil moisture is shown in terms of the 2015–2023 $RMSD$ with the stationary merging (Fig. 7). To remove the effect of differences in the intrinsic (location) variability, the value is expressed in terms of % of (stationary-merged) soil moisture standard deviation in the same period. Large parts of the domain show an impact of the seasonally-weighted merging of less than 10% of the original soil moisture variability, including most of Australia, the Great Plains region, India and central Asia, and most of Africa. However, a seasonal impact is observed in the croplands and grasslands of the Sahel region (DJF-MAM), in parts of southern Australia (JJA), in the mixed vegetation cover of the Horn of Africa (JJA) and Europe (DJF). The highest all-year impact is seen in the sparse vegetation and bare ground regions spanning from the Sahara desert to the Arabic peninsula (characterized by low intrinsic soil moisture variability) and in the needle-leaf forests in the Siberian and Canadian regions, and the Persian plateau. Here, the $RMSD$ in the soil moisture obtained with the two merging approaches is comparable to the standard deviation in the stationary-merged soil moisture data.

Overall, soil moisture estimates are not substantially changed by the seasonal merging. The changes observed in terms of $RMSD$ are generally both within the estimated uncertainty (for instance, the average estimated uncertainty over the in situ locations is $\sim 0.018 \quad m^3 * m^{-3}$) and below the empirical error found against the ground measurements (see Section 4.4). Furthermore, barely any difference is found in the global correlation ($R_{stationary} = 0.559$, $R_{seasonal} = 0.561$) and $ubRMSD$ ($ubRMSD_{stationary} = 0.040 \quad m^3 * m^{-3}$, $ubRMSD_{seasonal} = 0.039 \quad m^3 * m^{-3}$) against the in situ measurements (number of sensors $n = 3780$, median collocated observations per sensor $n = 873$, based on the dataset described in Section 2.3 and spatially and temporally collocated as described in Section 3.3).

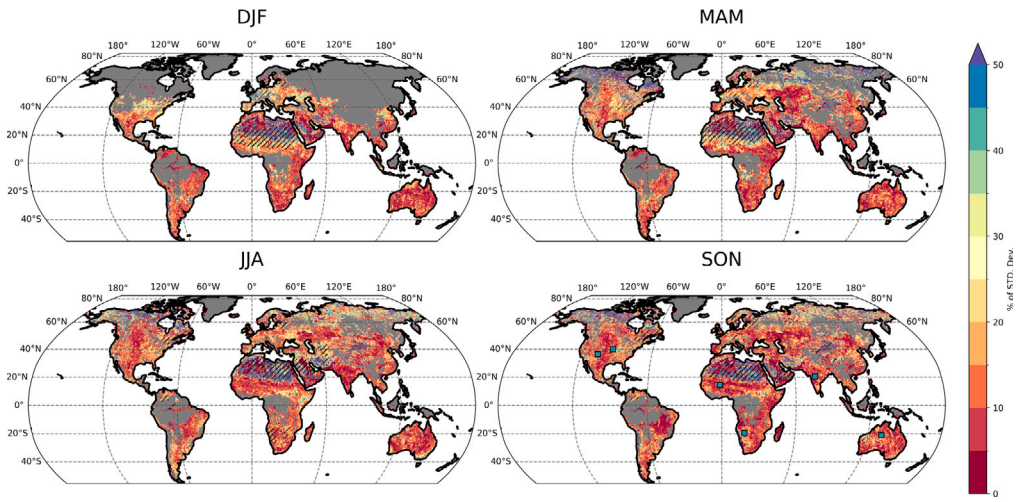

Fig. 7. $RMSD$ between the seasonally- and stationary-merged soil moisture products in % of (stationary-merged) soil moisture standard deviation, by season. Regions where the stationary-merged soil moisture standard deviation is smaller than the global 10th percentile are hatched. Gaps are due to masking of the soil moisture estimates where no retrieval is possible or where the quality is not assured and flagged, for example due to dense vegetation, frozen soil, permanent ice cover, or radio frequency interference. The points indicate the locations shown in Fig. 3.

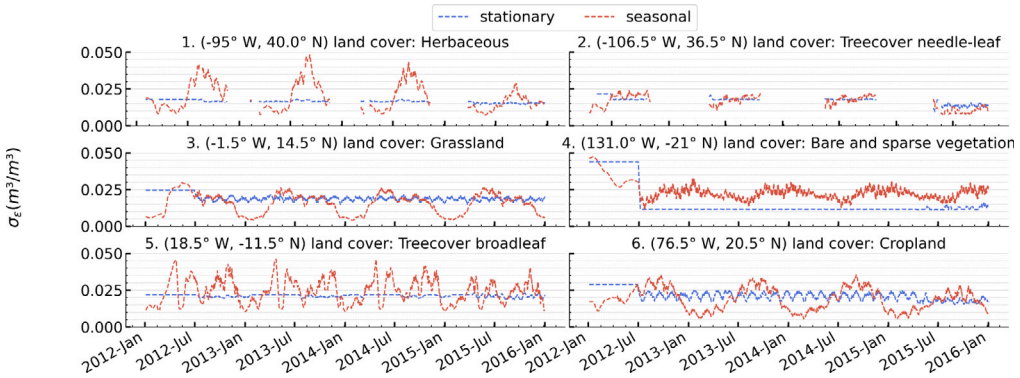

Fig. 8. Uncertainty of the seasonally- and stationary-merged soil moisture products for the points shown in Fig. 3. Based on aggregated ESA CCI Landcover classes described in Table A.3.

4.4. Uncertainty representation

Here, we evaluate the propagated seasonal uncertainties associated with the merged soil moisture and compare their agreement with uncertainty estimates derived using ground-based observations. With the stationary approach, the only variability in the uncertainty after propagation (Eq. (2)) is given by the number of sensors providing a valid observation, which varies over time due to different satellite orbits and sensor-inherent observation masking. Depending on the difference between their uncertainties, this can result in a more or less evident saw tooth profile (Fig. 8). Moreover, step-changes in the overall uncertainty level are caused by the addition of sensors, which occur in September 2012 (AMSR2) and April 2015 (SMAP). These features are inherent in the merging design and persist in the seasonal approach, but with a superposition of a climatological signal. The oscillation in the uncertainty is generally centred on the stationary estimates, but can sometimes be higher or lower reflecting the bias in the input uncertainties (Fig. A.14), as visible for instance at location (3), where the stationary uncertainty roughly provides the upper bound of the new uncertainty climatology, and (4), where on the contrary the new uncertainty is larger.

The bias in the TCA-based uncertainty estimates can be computed against the uncertainties estimated from in situ reference soil moisture $ubRMSD_{m,i}$ (Eq. (6)). In Fig. 9, the 2015–2023 $ubRMSD_{m,i}$ is compared with the mean σ_ϵ at all available in situ locations. For both seasonal and stationary σ_ϵ, the ratio is roughly log-normal and

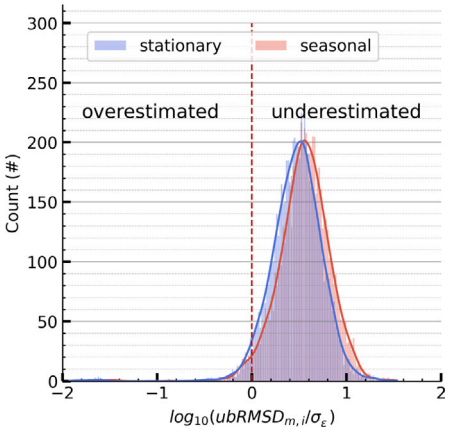

Fig. 9. Distribution of the uncertainty validation ratio for the seasonally- and stationary-merged soil moisture products.

offset from the centre, meaning that the uncertainty estimates are generally smaller compared to the reference soil moisture uncertainty for the seasonal and stationary approach alike. The underestimation is slightly larger for the seasonal merging, coherently with Fig. A.14. The closeness to a standard normal distribution for the (log-)ratio is also

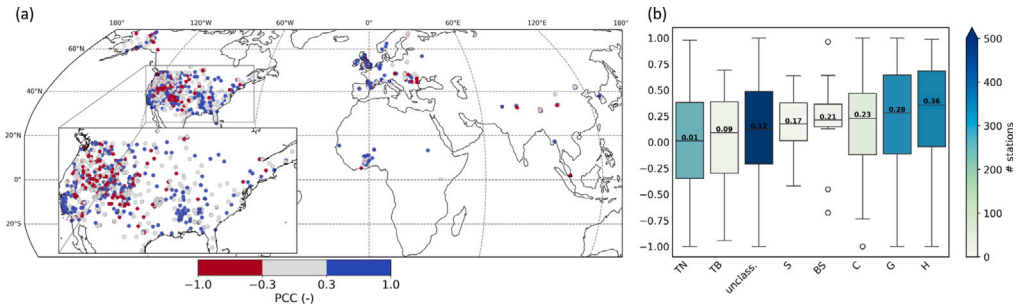

Fig. 10. Pearson R of the monthly ESA CCI SM error ($ubRMSD_{m,i}$) and estimated seasonal uncertainty (σ_ϵ) at each station in space (a), and (b) grouped by ESA CCI LC aggregated class.

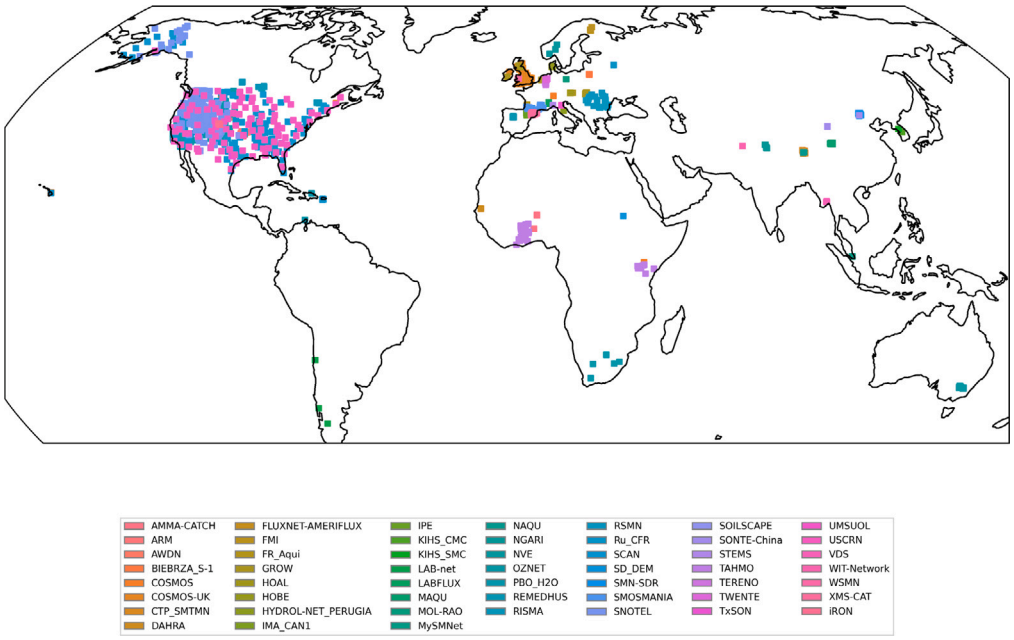

Fig. A.11. Location of the available ISMN sensors ($n = 3780$) and relative networks in the period 2015–2023 included in the $0 - 10$ cm depth.

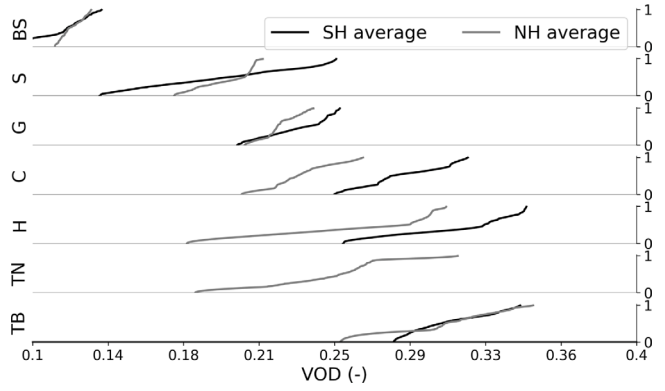

Fig. A.12. Cumulative distribution functions of the mean AMSR2 VOD climatology averaged over the ESACCI-landcover aggregated class (sampled per Northern and Southern Hemisphere).

considered a measure of accurate uncertainty (Merchant et al., 2017). In this case, the strong biases in the distributions compared to the 0 mean lead to a kurtosis of 7.4 and 9.7 for the seasonal and stationary products, respectively, which reflects an excess of outliers.

Overall, neither the stationary- nor seasonally-merged uncertainties are unbiased with respect to the ground-based uncertainty, and both appear to be underestimated over the sampled stations. In this respect, it should be pointed out that the uncertainty σ_ϵ^2 estimated with Eq. (2) is a measure of the random error variance in θ_m which does not consider possible static biases, and is relative to the data space of the scaling reference, GLDAS. The mean-standard deviation scaling of θ_m to the in situ data is intended to remove such biases. However, as previously noted (Gruber et al., 2020) this does not account for intrinsic differences in the signal-to-noise ratios of θ_m and θ_i, which leaves an additional error component in $ubRMSD_{m,i}$ compared to σ_ϵ. Such component can be intuitively understood as the instrumental noise of the ground sensors. In addition, the satellite product and the in situ measurements represent a different horizontal support, leading to a spatial scale random representativeness error (Gruber et al., 2013; Peng et al., 2025) which similarly contributes to the overall budget of $ubRMSD_{m,i}$. In other words, the $ubRMSD$ would essentially be a measure of the error standard deviation σ_ϵ only if the in situ measurement were a perfect representation of the soil moisture integrated over the satellite footprint, i.e., if the measurement and representativeness errors were removed. While this is not realistic in most cases (Miralles et al., 2010) – explaining at least in part the underestimation seen in Fig. 9 – in situ soil moisture is still considered the most reliable source of reference data (Dorigo et al., 2021). We did not attempt to mitigate the impact of these errors in the uncertainty validation, for instance by limiting the in situ selection to fiducial reference measurements (FRMs) (Goryl et al., 2023). Firstly, because proposed FRMs indicators are generally

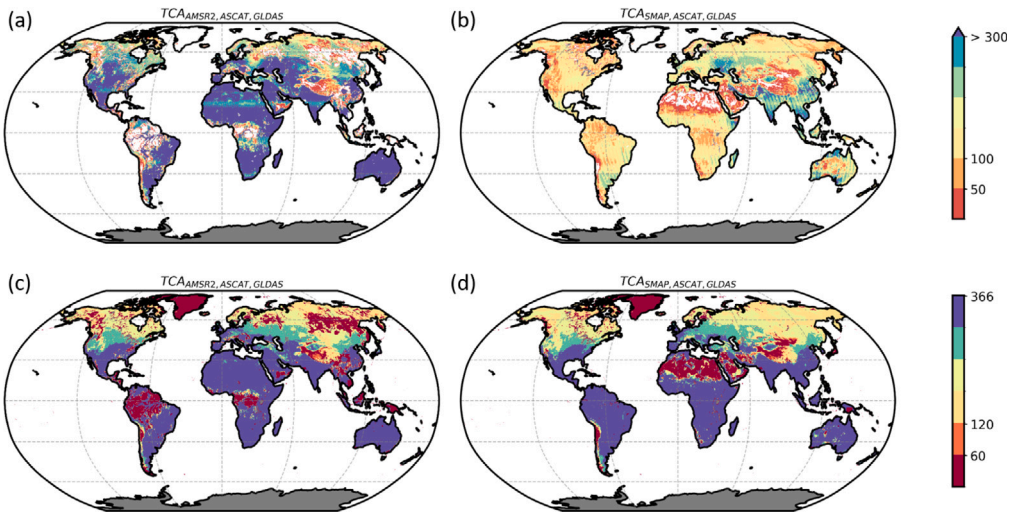

Fig. A.13. (a), (b) Average sample size for 366 climatological windows over the period 2015–2023 (c), (d) number of climatological windows with at least 30 valid observations over the period 2015–2023.

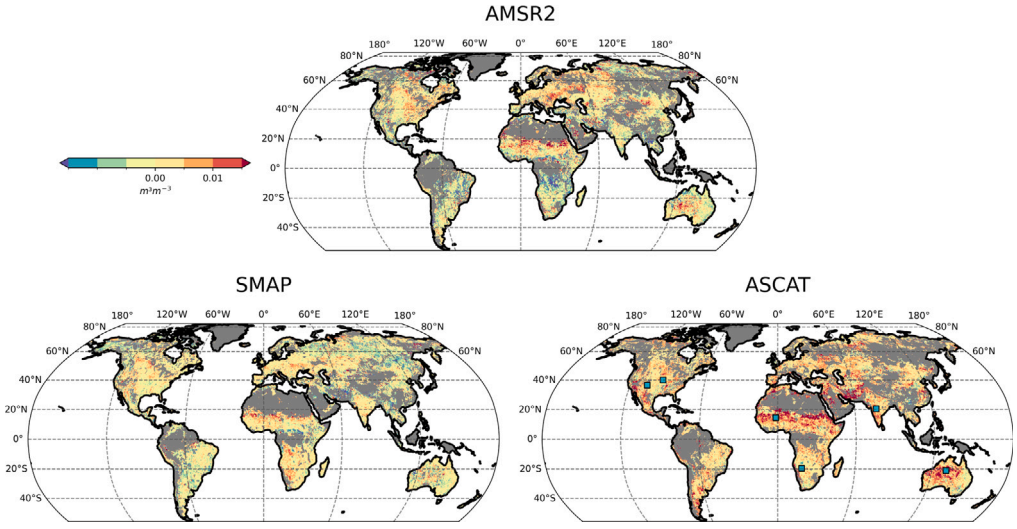

Fig. A.14. Difference of the stationary uncertainty and the median of the soil moisture uncertainty climatology for the input products after gap-filling through uncertainty/VOD regression. Gaps are due to too few collocated data and *p-value* masking.

inferred from a comparison with satellite based soil moisture (Gruber et al., 2013), which may lead to a confirmation bias in the comparison of $ubRMSD$ and σ_ϵ. Secondly, because errors in situ measurements affect the validation scores for the stationary and seasonally merged products in equal measure, and – in terms of evaluating the potential improvement in the new uncertainty representation – can be neglected.

Overall, temporal dynamics in the new soil moisture uncertainty match with the inter-seasonal dynamics of $ubRMSD_{m,i}$. The correlation between the two at monthly aggregation (which limits the impact of sensor availability-driven σ_ϵ variability) results in a global (i.e., considering all ISMN sensors) median R of 0.19, with 720 sensors (42% of the total) with $R > 0.3$.

Fig. 10a shows that the correlation has an evident, although not clearly delimited, regional connotation. Notable negative correlations ($R \leq -0.3$) are especially clustered in the western forested mountains of the United States and in Europe over the Romanian RSMN network. Negligible correlations ($-0.3 < R < 0.3$) are generally more scattered and homogeneously distributed between the area of negative R and the West–East divide of the United States. Notable positive correlations ($R \geq 0.3$) are grouped in the South-East and South-West of the United States, in most European Networks and especially COSMOS-UK and REMEDHUS, and in the West African TAHMO Network. It should be noted that the ISMN is subject to a evident geographic sampling bias. Therefore, it is difficult to interpret the observed spatial patterns robustly. However, the results sufficiently show that the new uncertainty representation can be consistent with in situ estimates – at least in terms of seasonality – depending on some spatial land surface characteristics. LC itself does not entirely explain such consistency, with only a small separation between the worst ($R_{TN} = 0.01$) and best correlated ($R_H = 0.36$, weak positive) classes, and all showing a wide IQR (Fig. 10b). A better separation is observed when classifying the sensors by network (Fig. A.15). Considering that the in situ measurements also show distinct error regimes mainly by network (Gruber et al., 2013), this may at least in part explain the variability in correlation seen between the predicted uncertainty and the in situ based error, given that the in situ uncertainty is part of the $ubRMSD_{m,i}$ error budget. The natural absence of strong seasonalities in the uncertainty in large parts of the NH (see Fig. 2), where most of the ISMN stations are located, may also cause the (de-)correlation to be mainly driven by sampling-related estimation errors in $ubRMSD_{m,i}$ and σ_ϵ.

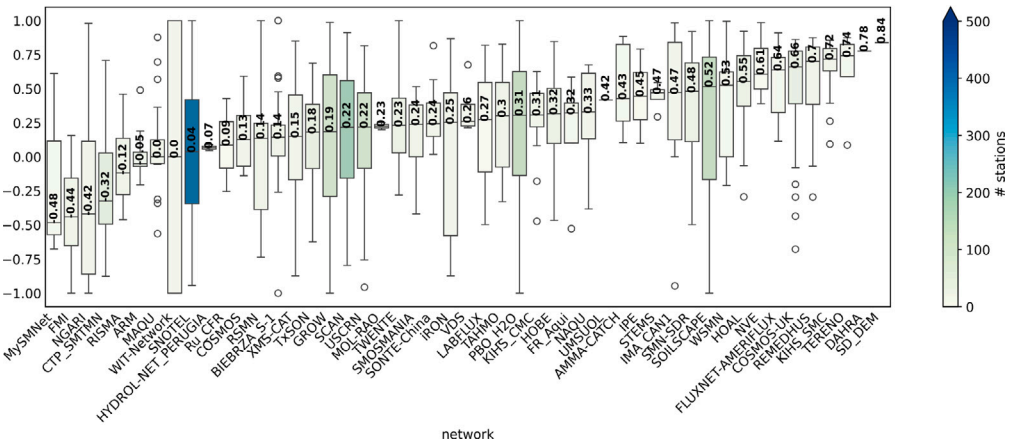

Fig. A.15. As Fig. 10b, but classified by ISMN network.

5. Conclusions and outlook

In this study, we evaluated an alternative merging strategy for multi-satellite soil moisture records, which implicitly accounts for seasonal sources of uncertainty. To do so, we characterized the uncertainty of three satellite input products with a seasonal modification of TCA to obtain a climatology of error variance and (inversely proportional) merging weight estimates. We used in situ soil moisture measurements to evaluate the reliability of the provided uncertainty field. We further stratified the results using a land cover classification that strongly connotates different vegetation regimes by mean and variability, based on the expectation that vegetation characteristics are the main drivers of uncertainty in soil moisture retrievals.

In line with previous efforts, we found strong fluctuations in the uncertainty climatologies of satellite SM retrievals. Such fluctuations are generally consistent between the studied sensors – particularly between the two passive sensors AMSR2 and SMAP – leading to limited deviations in the seasonal weights compared to the static weights. The strongest seasonalities in the merging weights over the Southern Hemisphere (where there are less data gaps than over the Northern Hemisphere) are observed for the shrubland and herbaceous land cover types, and no clear relation of the weights seasonalities to the strength of the intra-annual vegetation cycle or mean vegetation conditions is identified.

When using the seasonal uncertainty information in the merging, the temporal consistency between the sensors' uncertainty over time leads to only minor changes in the merged soil moisture product compared to the static case. Despite this, the uncertainty field provided with the product is now connotated with a strong climatological component, which was previously unaccounted for. Net of an underestimation in its magnitude – which is also present for the stationary merged uncertainty – the new uncertainty agrees reasonably well with the in situ-based uncertainty in terms of correlation, increasing the confidence in its ability to realistically represent the error budget of the observations.

The adaptation of TCA suits the stated aim to improve the representation of uncertainty in CDRs, and could be achieved without necessity of additional data. Based on the above results, we find recommendable to account for the seasonal component of retrieval uncertainty – rather than its stationary value alone – in the context of error-informed data merging. Not only where, but also when, is the data reliable is an important piece of the uncertainty information which can lead to more meaningful Earth Observation-based data and better decision making (Gruber et al., 2025).

In terms of applicability, the method is limited by the availability of valid observations in the pre-defined temporal subsets. This implies that a different temporal definition, by changing either the windowing frequency or its size, could be more suitable for example in shorter data records. Based on this, we identify the retrieval of information on the stability of the uncertainty estimates in the merging as a logical next step towards finding the optimal trade-off between the temporal information carried in the uncertainty and its precision. Moreover, we strongly advocate for continued research in this field – particularly in the merging of higher-resolution soil moisture products. Here, the proposed approach becomes especially relevant due to more pronounced local-scale differences in surface conditions which affect the parameterization of the retrieval in return.

CRediT authorship contribution statement

Pietro Stradiotti: Writing – original draft, Formal analysis, Data curation, Conceptualization. **Alexander Gruber:** Writing – review & editing, Conceptualization. **Wolfgang Preimesberger:** Writing – review & editing, Software, Data curation. **Wouter Dorigo:** Writing – review & editing, Supervision, Funding acquisition.

Funding statement

This dataset was produced with funding from the European Space Agency (ESA) Climate Change Initiative (CCI) Plus Soil Moisture Project (CCN 3 to ESRIN Contract No: 4000126684/19/I-NB "ESA CCI+ Phase 1 New R&D on CCI ECVS Soil Moisture").

The authors acknowledge TU Wien Bibliothek, Austria for financial support through its Open Access Funding Programme.

Declaration of competing interest

The authors declare that they have no known competing financial interests or personal relationships that could have appeared to influence the work reported in this paper.

Appendix. Supplementary information

See Figs. A.11–A.15 and Tables A.2 and A.3.

Data availability

The processed data required to reproduce the above findings are available at https://doi.org/10.48436/z0zzp-f4j39 and can be cited with Stradiotti et al. (2025).

Table A.2
References to the ISMN Networks used in the study.

AMMA-CATCH	Pellarin et al. (2009), Mougin et al. (2009), Cappelaere et al. (2009), Rosnay et al. (2009), Lebel et al. (2009), Galle et al. (2015)
ARM	Cook, 2018)
BIEBRZA S-1	Musial et al. (2016)
COSMOS	Zreda et al. (2008, 2012)
COSMOS UK	–
CTP_SMTMN	Yang et al. (2013)
DAHRA	Tagesson et al. (2014)
FLUXNET-AMERIFLUX	–
FMI	Ikonen et al., 2016)
FR_Aqui	Al-Yaari et al. (2018), Wigneron et al. (2018)
GROW	Xaver et al. (2020), Zappa et al. (2019, 2020)
HOAL	Blöschl et al. (2016), Vreugdenhil et al. (2013)
HOBE	Bircher et al. (2012), Jensen and Refsgaard (2018)
HYDROL-NET PERUGIA	Hollinger and Isard (1994)
IMA_CAN1	Biddoccu et al. (2016), Capello et al. (2019a), Raffelli et al. (2017)
IPE	Alday et al. (2020)
KIHS_CMC	–
KIHS_SMC	–
LAB-net	Mattar et al. (2016, 2014)
LABFLUX	–
MAQU	Su et al. (2011), Dente et al. (2012)
MySMNet	Kang et al. (2019)
MOL-RAO	Beyrich and Adam (2007)
NAQU	Su et al. (2011), Dente et al. (2012)
NGARI	Su et al. (2011), Dente et al. (2012)
NVE	–
OZNET	Smith et al. (2012), Young et al. (2008)
PBO_H20	Larson et al. (2008)
REMEDHUS	González-Zamora et al. (2019)
RISMA	Ojo et al. (2015), L'Heureux (2011), Canisius (2011)
RSMN	–
SCAN	Schaefer et al. (2007)
SD_DEM	Ardö (2013)
SMN-SDR	Zhao et al. (2020), Zheng et al. (2022)
SMOSMANIA	Calvet et al. (2016), Albergel et al. (2008), Calvet et al. (2007)
SNOTEL	Leavesley et al. (2008), Leavesleys (2010)
SOILSCAPE	Moghaddam et al. (2011, 2016), Shuman et al. (2010)
SONTE-China	–
STEMS	Capello et al. (2019a), Darouich et al. (2022)
TAHMO	–
TERENO	Zacharias et al. (2011), Bogena et al. (2018, 2012), Bogena (2016)
TWENTE	–
TxSON	–
UMSUOL	–
USCRN	Bell et al. (2013)
VDS	–
WIT-Network	–
WSMN	Petropoulos and McCalmont (2017)
XMS-CAT	–
iRON	Osenga et al. (2021, 2019)

Table A.3
Lookup table of the ESACCI-landcover classes to the thematic grouping used to stratify the results.

Acronym	Thematic grouping	ESACCI-landcover classes
BS	Bare and sparse vegetation	200, 150, 152, 153
S	Shrubland	12, 100, 120, 121, 122
H	Herbacous	11, 110
G	Grassland	130
C	Cropland	10, 20, 30
TB	Treecover, broadleaf	50, 62
TN	Treecover, needle-leaf	70, 82

References

Al-Yaari, A., Dayau, S., Chipeaux, C., Aluome, C., Kruszewski, A., Loustau, D., Wigneron, J.-P., 2018. The AQUI soil moisture network for satellite microwave remote sensing validation in South-Western France. Remote. Sens. 10 (11), http://dx.doi.org/10.3390/rs10111839, article 1839.

Albergel, C., Rüdiger, C., Pellarin, T., Calvet, J.-C., Fritz, N., Froissard, F., Suquia, D., Petitpa, A., Piguet, B., Martin, E., 2008. From near-surface to root-zone soil moisture using an exponential filter: an assessment of the method based on in-situ observations and model simulations. Hydrol. Earth Syst. Sci. 12 (6), 1323–1337. http://dx.doi.org/10.5194/hess-12-1323-2008.

Alday, J.G., Camarero, J.J., Revilla, J., Resco de Dios, V., 2020. Similar diurnal, seasonal and annual rhythms in radial root expansion across two coexisting mediterranean oak species. Tree Physiol. 40 (7), 956–968. http://dx.doi.org/10.1093/treephys/tpaa041.

Ardö, J., 2013. A 10-year dataset of basic meteorology and soil properties in Central Sudan. In: Dataset Papers in Geosciences, vol. 2013, http://dx.doi.org/10.7167/2013/297973/dataset.

Bell, J., Palecki, M., Baker, B., Collins, W., Lawrimore, J., Leeper, R., Hall, M., Kochendorfer, J., Meyers, T., Wilson, T., Diamond, H., 2013. U.S. climate reference network soil moisture and temperature observations. J. Hydrometeorol. 14, 977–988. http://dx.doi.org/10.1175/JHM-D-12-0146.1.

Beyrich, F., Adam, W.K., 2007. Site and data report for the lindenberg reference site in CEOP - phase 1. In: Berichte des Deutschen Wetterdienstes, vol. 230, Offenbach am Main, p. 2007.

Biddoccu, M., Ferraris, S., Opsi, F., Cavallo, E., 2016. Long-term monitoring of soil management effects on runoff and soil erosion in sloping vineyards in Alto Monferrato (North West Italy). Soil Tillage Res. 155, 176–189. http://dx.doi.org/10.1016/j.still.2015.07.005.

Bircher, S., Skou, N., Jensen, K., Walker, J., Rasmussen, L., 2012. A soil moisture and temperature network for SMOS validation in western Denmark. Hydrol. Earth Syst. Sci. 16, http://dx.doi.org/10.5194/hess-16-1445-2012.

Blöschl, G., Blaschke, A.P., Broer, M., Bucher, C., Carr, G., Chen, X., Eder, A., Exner-Kittridge, M., Farnleitner, A., Flores-Orozco, A., Haas, P., Hogan, P., Kazemi Amiri, A., Oismüller, M., Parajka, J., Silasari, R., Stadler, P., Strauss, P., Vreugdenhil, M., Wagner, W., Zessner, M., 2016. The hydrological open air laboratory (HOAL) in Petzenkirchen: a hypothesis-driven observatory. Hydrol. Earth Syst. Sci. 20 (1), 227–255. http://dx.doi.org/10.5194/hess-20-227-2016.

Bogena, H.R., 2016. TERENO: German network of terrestrial environmental observatories. J. Large- Scale Res. Facil. 2, A52. http://dx.doi.org/10.17815/jlsrf-2-98.

Bogena, H., Kunkel, R., Pütz, T., Vereecken, H., Kruger, E., Zacharias, S., Dietrich, P., Wollschläger, U., Kunstmann, H., Papen, H., Schmid, H., Munch, J., Priesack, E., Schwank, M., Bens, O., Brauer, A., Borg, E., Hajnsek, I., 2012. TERENO - long-term monitoring network for terrestrial environmental research. In: Hydrologie Und Wasserbewirtschaftung, vol. 56, pp. 138–143.

Bogena, H.R., Montzka, C., Huisman, J.A., Graf, A., Schmidt, M., Stockinger, M., von Hebel, C., Hendricks-Franssen, H.J., van der Kruk, J., Tappe, W., Lücke, A., Baatz, R., Bol, R., Groh, J., Pütz, T., Jakobi, J., Kunkel, R., Sorg, J., Vereecken, H., 2018. The TERENO-rur hydrological observatory: A multiscale multi-compartment research platform for the advancement of hydrological science. Vadose Zone J. 17 (1), 180055. http://dx.doi.org/10.2136/vzj2018.03.0055.

Brocca, L., Hasenauer, S., Lacava, T., Melone, F., Moramarco, T., Wagner, W., Dorigo, W., Matgen, P., Martínez-Fernández, J., Llorens, P., Latron, J., Martin, C., Bittelli, M., 2011. Soil moisture estimation through ASCAT and AMSR-Esensors: An intercomparison and validation study across Europe. Remote Sens. Environ. 115 (12), 3390–3408. http://dx.doi.org/10.1016/j.rse.2011.08.003.

Calvet, J.-C., Fritz, N., Berne, C., Piguet, B., Maurel, W., Meurey, C., 2016. Deriving pedotransfer functions for soil quartz fraction in southern France from reverse modeling. SOIL 2 (4), 615–629. http://dx.doi.org/10.5194/soil-2-615-2016.

Calvet, J.-C., Fritz, N., Froissard, F., Suquia, D., Petitpa, A., Piguet, B., 2007. In situ soil moisture observations for the CAL/VAL of SMOS: the SMOSMANIA network. In: 2007 IEEE International Geoscience and Remote Sensing Symposium. pp. 1196–1199. http://dx.doi.org/10.1109/IGARSS.2007.4423019.

Canisius, F., 2011. Calibration of Casselman, Ontario soil moisture monitoring network. In: Agriculture and Agri-Food Canada. Ottawa, ON, p. 37.

Capello, G., Biddoccu, M., Ferraris, S., Cavallo, E., 2019a. Effects of tractor passes on hydrological and soil erosion processes in tilled and grassed vineyards. Water 11 (10), 2118. http://dx.doi.org/10.3390/w11102118.

Cappelaere, B., Descroix, L., Lebel, T., Boulain, N., Ramier, D., Laurent, J.-P., Favreau, G., Boubkraoui, S., Boucher, M., Moussa, I., et al., 2009. The AMMA-CATCH experiment in the cultivated sahelian area of south-west Niger: Investigating water cycle response to a fluctuating climate and changing environment. J. Hydrol. 375, 34–51. http://dx.doi.org/10.1016/j.jhydrol.2009.06.021.

Cook, D.R., Soil Temperature and Moisture Profile (STAMP) System Handbook. United States, http://dx.doi.org/10.2172/1332724.

Cook, D.R., 2018. Surface Energy Balance System (SEBS) Instrument Handbook. United States, http://dx.doi.org/10.2172/1004944.

Darouich, H., Ramos, T.B., Pereira, L.S., Rabino, D., Bagagiolo, G., Capello, G., Simionesei, L., Cavallo, E., Biddoccu, M., 2022. Water use and soil water balance of Mediterranean vineyards under rainfed and drip irrigation management: Evapotranspiration partition and soil management modelling for resource conservation. Water 14 (4), 554. http://dx.doi.org/10.3390/w14040554.

de Nijs, A.H.A., Parinussa, R.M., de Jeu, R.A.M., Schellekens, J., Holmes, T.R.H., 2015. A methodology to determine radio-frequency interference in AMSR2 observations. IEEE Trans. Geosci. Remote. Sensing 53 (9), 5148–5159. http://dx.doi.org/10.1109/TGRS.2015.2417653.

Dente, L., Su, Z., Wen, J., 2012. Validation of SMOS soil moisture products over the Maqu and Twente regions. Sensors 12 (8), 9965–9986.

Dorigo, W., Himmelbauer, I., Aberer, D., Schremmer, L., Petrakovic, I., Zappa, L., Preimesberger, W., Xaver, A., Annor, F., Ardö, J., et al., 2021. The international soil moisture network: serving earth system science for over a decade. Hydrol. Earth Syst. Sci. 25 (11), 5749–5804.

Dorigo, W., Preimesberger, W., Stradiotti, P., Kidd, R., van der Schalie, R., van der Vliet, M., Rodriguez-Fernandez, N., Madelon, R., Baghdadi, N., 2023. ESA climate change initiative plus - soil moisture algorithm theoretical baseline document (ATBD) supporting product version 08.1 (version 1.1), Zenodo. http://dx.doi.org/10.5281/zenodo.8320869.

Dorigo, W.A., Scipal, K., Parinussa, R.M., Liu, Y.Y., Wagner, W., de Jeu, R.A.M., Naeimi, V., 2010. Error characterisation of global active and passive microwave soil moisture datasets. Hydrol. Earth Syst. Sci. 14 (12), 2605–2616. http://dx.doi.org/10.5194/hess-14-2605-2010.

Dorigo, W., Wagner, W., Albergel, C., Albrecht, F., Balsamo, G., Brocca, L., Chung, D., Ertl, M., Forkel, M., Gruber, A., Haas, E., Hamer, P.D., Hirschi, M., Ikonen, J., de Jeu, R., Kidd. W. Lahoz, R., Liu, Y.Y., Miralles, D., Mistelbauer, T., Nicolai-Shaw, N., Parinussa, R., Pratola, C., Reimer, C., van der Schalie, R., Seneviratne, S.I., Smolander, T., Lecomte, P., 2017. ESA CCI soil moisture for improved Earth system understanding: State-of-the art and future directions. Remote Sens. Environ. 203, 185–215.

Dorigo, W.A., Xaver, A., Vreugdenhil, M., Gruber, A., Hegyiova, A., Sanchis-Dufau, A.D., Zamojski, D., Cordes, C., Wagner, W., Drusch, M., 2013. Global automated quality control of in situ soil moisture data from the international soil moisture network. Vadose Zone J. 12 (3), article vzj, The Soil Science Society of America, Inc.

Draper, C., Reichle, R., de Jeu, R., Naeimi, V., Parinussa, R., Wagner, W., 2013. Estimating root mean square errors in remotely sensed soil moisture over continental scale domains. Remote Sens. Environ. 137, 288–298. http://dx.doi.org/10.1016/j.rse.2013.06.013.

E.S.A. Land Cover C.C.I. project team, Defourny, P., 2019. ESA Land Cover Climate Change Initiative (Land_Cover_cci): Global Land Cover Maps, Version 2.0.7, Centre for Environmental Data Analysis. [Online]. Available: https://catalogue.ceda.ac.uk/uuid/b382ebe6679d44b8b0e68ea4ef4b701c/. (Accessed 27 September 2024).

Formanek, M., Gruber, A., Stradiotti, P., Dorigo, W., 2025. What is the uncertainty of the uncertainty and (why) does it matter? Improving the uncertainty estimates of merged multi-satellite soil moisture data sets. Surv. Geophys. submitted for publication.

Galle, S., Grippa, M., Peugeot, C., Bouzou Moussa, I., Cappelaere, B., Demarty, J., Mougin, E., Lebel, T., Chaffard, V., 2015. AMMA-CATCH: A hydrological, meteorological and ecological long term observatory on West Africa: Some recent results. AGU Fall Meet. Abstr. 2015, paper GC42A-01.

González-Zamora, Á., Sánchez, N., Pablos, M., Martínez-Fernández, J., 2019. CCI soil moisture assessment with SMOS soil moisture and in situ data under different environmental conditions and spatial scales in Spain. Remote Sens. Environ. 225, 469–482. http://dx.doi.org/10.1016/j.rse.2018.02.010.

Goryl, P., Fox, N., Donlon, C., Castracane, P., 2023. Fiducial reference measurements (FRMs): What are they? Remote. Sens. 15 (20), http://dx.doi.org/10.3390/rs15205017, article 5017.

Gruber, A., Bulgin, C.E., Dorigo, W., Embury, O., Formanek, M., Merchant, C., Mittaz, J., Muñoz-Sabater, J., Pöppl, F., Povey, A., Wagner, W., 2025. Making sense of uncertainties: Ask the right question. Surv. Geophys. http://dx.doi.org/10.1007/s10712-025-09889-5.

Gruber, A., De Lannoy, G., Albergel, C., Al-Yaari, A., Brocca, L., Calvet, J.-C., Colliander, A., Cosh, M., Crow, W., Dorigo, W., Draper, C., Hirschi, M., Kerr, Y., Konings, A., Lahoz, W., McColl, K., Montzka, C., Muñoz-Sabater, J., Peng, J., Reichle, R., Richaume, P., Rüdiger, C., Scanlon, T., van der Schalie, R., Wigneron, J.-P., Wagner, W., 2020. Validation practices for satellite soil moisture retrievals: What are (the) errors? Remote Sens. Environ. 244, 111806. http://dx.doi.org/10.1016/j.rse.2020.111806.

Gruber, A., Dorigo, W.A., Crow, W., Wagner, W., 2017. Triple collocation-based merging of satellite soil moisture retrievals. IEEE Trans. Geosci. Remote Sens. 55 (12), 6780–6792. http://dx.doi.org/10.1109/TGRS.2017.2734070.

Gruber, A., Dorigo, W.A., Zwieback, S., Xaver, A., Wagner, W., 2013. Characterizing coarse-scale representativeness of in situ soil moisture measurements from the international soil moisture network. Vadose Zone J. 12 (2), 1–16.

Gruber, A., Scanlon, T., van der Schalie, R., Wagner, W., Dorigo, W., 2019. Evolution of the ESA CCI SM climate data records and their underlying merging methodology. Earth Syst. Sci. Data 11 (2), 717–739.

Gruber, A., Su, C.-H., Zwieback, S., Crow, W., Dorigo, W., Wagner, W., 2016. Recent advances in (soil moisture) triple collocation analysis. Int. J. Appl. Earth Obs. Geoinf. 45, 200–211. http://dx.doi.org/10.1016/j.jag.2015.09.002, Here is the reformatted version of your citations in the requested format.

Hollinger, S., Isard, S., 1994. A soil moisture climatology of illinois. J. Clim. 7, 822–833. http://dx.doi.org/10.1175/1520-0442(1994)007<0822:ASMCOI>2.0.CO;2.

Ikonen, J., Smolander, T., Rautiainen, K., Cohen, J., Lemmetyinen, J., Salminen, M., Pulliainen, J., Spatially distributed evaluation of ESA CCI soil moisture products in a northern boreal forest environment. Geosciences 8 (2), 2018. http://dx.doi.org/10.3390/geosciences8020051, article 51.

Ikonen, J., Vehviläinen, J., Rautiainen, K., Smolander, T., Lemmetyinen, J., Bircher, S., Pulliainen, J., 2016. The sodankylä in-situ soil moisture observation network: an example application to earth observation data product evaluation. Geosci. Instrum. Methods Data Syst. 5 (1), 95–108. http://dx.doi.org/10.5194/gi-5-95-2016.

Jensen, K.H., Refsgaard, J.C., 2018. HOBE: The Danish hydrological observatory. Vadose Zone J. 17 (1), http://dx.doi.org/10.2136/vzj2018.03.0059, article 180059.

Kang, C.S., Kanniah, K.D., Kerr, Y.H., 2019. Calibration of SMOS soil moisture retrieval algorithm: A case of tropical site in Malaysia. IEEE Trans. Geosci. Remote Sens. 57 (6), 3827–3839. http://dx.doi.org/10.1109/TGRS.2019.2898378.

Kerr, Y.H., Waldteufel, P., Wigneron, J.-P., Delwart, S., Cabot, F., Boutin, J., Escorihuela, M.-J., Font, J., Reul, N., Gruhier, C., Juglea, S.E., Drinkwater, M.R., Hahne, A., Martín-Neira, M., Mecklenburg, S., 2010. The SMOS mission: New tool for monitoring key elements of the global water cycle. Proc. IEEE 98 (5), 666–687. http://dx.doi.org/10.1109/JPROC.2010.2043032.

Kim, H., Parinussa, R., Konings, A.G., Wagner, W., Cosh, M.H., Lakshmi, V., Zohaib, M., Choi, M., 2018. Global-scale assessment and combination of SMAP with ASCAT (active) and AMSR2 (passive) soil moisture products. Remote Sens. Environ. 204, 260–275. http://dx.doi.org/10.1016/j.rse.2017.10.026.

Kim, S., Parinussa, R.M., Liu, Y.Y., Johnson, F.M., Sharma, A., 2016. Merging alternate remotely-sensed soil moisture retrievals using a non-stationary model combination approach. Remote. Sens. 8 (6), 518. http://dx.doi.org/10.3390/rs8060518.

Larson, K., Small, E., Gutmann, E., Bilich, A., Braun, J., Zavorotny, V., Larson, C., 2008. Use of GPS receivers as a soil moisture network for water cycle studies. Geophys. Res. Lett. 35 (24), http://dx.doi.org/10.1029/2008GL036013.

Leavesley, G.H., David, O., Garen, D.C., Lea, J., Marron, J.K., Pagano, T.C., Perkins, T.R., Strobel, M.L., 2008. A modeling framework for improved agricultural water supply forecasting. In: AGU Fall Meeting Abstracts, vol. 2008, pp. C21A–0497.

Leavesleys, G.H., 2010. A modelling framework for improved agricultural water-supply forecasting.

Lebel, T., Cappelaere, B., Galle, S., Hanan, N., Kergoat, L., Levis, S., Vieux, B., Descroix, L., Gosset, M., Mougin, E., et al., 2009. AMMA-CATCH studies in the Sahelian region of West Africa: an overview. J. Hydrol. 375, 3–13. http://dx.doi.org/10.1016/j.jhydrol.2009.03.020.

L'Heureux, J., 2011. 2011 installation report for AAFC-SAGES soil moisture stations in Kenaston. SK. Agriculture.

Liu, Y.Y., Parinussa, R.M., Dorigo, W.A., De Jeu, R.A.M., Wagner, W., van Dijk, A.I.J.M., McCabe, M.F., Evans, J.P., 2011. Developing an improved soil moisture dataset by blending passive and active microwave satellite-based retrievals. Hydrol. Earth Syst. Sci. 15 (2), 425–436. http://dx.doi.org/10.5194/hess-15-425-2011.

Loew, A., Schlenz, F., 2011. A dynamic approach for evaluating coarse scale satellite soil moisture products. Hydrol. Earth Syst. Sci. 15 (1), 75–90. http://dx.doi.org/10.5194/hess-15-75-2011.

Mattar, C., Santamaría-Artigas, A., Durán-Alarcón, C., Olivera-Guerra, L., Fuster, R., 2014. LAB-net: the first Chilean soil moisture network for remote sensing applications. In: Quantitative Remote Sensing Symposium. RAQRS, pp. 22–26.

Mattar, C., Santamaría-Artigas, A., Durán-Alarcón, C., Olivera-Guerra, L., Fuster, R., Borvarán, D., 2016. The LAB-net soil moisture network: Application to thermal remote sensing and surface energy balance. Data 1 (1), http://dx.doi.org/10.3390/data1010006, article 6.

Merchant, C.J., Paul, F., Popp, T., Ablain, M., Bontemps, S., Defourny, P., Hollmann, R., Lavergne, T., Laeng, A., de Leeuw, G., et al., 2017. Uncertainty information in climate data records from Earth observation. Earth Syst. Sci. Data 9 (2), 511–527.

Miralles, D.G., Crow, W.T., Cosh, M.H., 2010. Estimating spatial sampling errors in coarse-scale soil moisture estimates derived from point-scale observations. J. Hydrometeorol. 11 (6), 1423–1429. http://dx.doi.org/10.1175/2010JHM1285.1.

Moesinger, L., Dorigo, W., de Jeu, R., van der Schalie, R., Scanlon, T., Teubner, I., Forkel, M., 2020. The global long-term microwave vegetation optical depth climate archive (VODCA). Earth Syst. Sci. Data 12 (1), 177–196. http://dx.doi.org/10.5194/essd-12-177-2020.

Moghaddam, M., Entekhabi, D., Goykhman, Y., Li, K., Liu, M., Mahajan, A., Nayyar, A., Shuman, D., Teneketzis, D., 2011. A wireless soil moisture smart sensor web using physics-based optimal control: Concept and initial demonstrations. IEEE J. Sel. Top. Appl. Earth Obs. Remote. Sens. 3 (4), 522–535. http://dx.doi.org/10.1109/JSTARS.2010.2052918.

Moghaddam, M., Silva, A., Clewley, D., Akbar, R., Hussaini, S.A., Whitcomb, J., Devarakonda, R., Shrestha, R., Cook, R.B., Prakash, G., Santhana Vannan, S.K., Boyer, A.G., 2016. Soil Moisture Profiles and Temperature Data from SoilSCAPE Sites. ORNL Distributed Active Archive Center, USA, http://dx.doi.org/10.3334/ORNLDAAC/1339.

Mougin, E., Hiernaux, P., Kergoat, L., Grippa, M., Rosnay, P., Timouk, F., Le Dantec, V., Demarez, V., Lavenu, F., Arjounin, M., et al., 2009. The AMMA-CATCH Gourma observatory site in Mali: Relating climatic variations to changes in vegetation, surface hydrology, fluxes and natural resources. J. Hydrol. 375, http://dx.doi.org/10.1016/j.jhydrol.2009.06.045.

Musial, J.P., Dabrowska-Zielinska, K., Kiryla, W., Oleszczuk, R., Gnatowski, T., Jaszczynski, J., 2016. Derivation and validation of the high resolution satellite soil moisture products: a case study of the Biebrza Sentinel-1 validation sites. Geoinf. Issues 8 (1), 37–53, 8.

Naeimi, V., Scipal, K., Bartalis, Z., Hasenauer, S., Wagner, W., 2009. An improved soil moisture retrieval algorithm for ERS and METOP scatterometer observations. IEEE Trans. Geosci. Remote Sens. 47 (7), 1999–2013. http://dx.doi.org/10.1109/TGRS.2008.2011617.

Notz, D., 2015. How well must climate models agree with observations? Philos. Trans. R. Soc. A: Math. Phys. Eng. Sci. 373, 20140164. http://dx.doi.org/10.1098/rsta.2014.0164.

Ojo, E.R., Bullock, P., Heureux, J.L., Powers, J., McNairn, H., Pacheco, A., 2015. Calibration and evaluation of a frequency domain reflectometry sensor for real-time soil moisture monitoring. Vadose Zone J. 14 (3), http://dx.doi.org/10.2136/vzj2014.08.0114.

Osenga, E.C., Arnott, J.C., Endsley, K.A., Katzenberger, J.W., 2019. Bioclimatic and soil moisture monitoring across elevation in a mountain watershed: Opportunities for research and resource management. Water Resour. Res. 55 (3), 2493–2503. http://dx.doi.org/10.1029/2018WR023653.

Osenga, E.C., Vano, J.A., Arnott, J.C., 2021. A community-supported weather and soil moisture monitoring database of the roaring fork catchment of the Colorado river headwaters. Hydrol. Process. 35 (3), e14081.

Owe, M., de Jeu, R., Holmes, T., 2008. Multisensor historical climatology of satellite-derived global land surface moisture. J. Geophys. Res.: Earth Surf. 113 (1), http://dx.doi.org/10.1029/2007JF000769.

Parinussa, R.M., De Jeu, R.A.M., Van der Schalie, R., Crow, W.T., Lei, F., Holmes, T.R.H., A quasi-global approach to improve day-time satellite surface soil moisture anomalies through the land surface temperature input. Climate 4 (4), 2016. http://dx.doi.org/10.3390/cli4040050, Art. 50.

Parinussa, R.M., Meesters, A.G.C.A., Liu, Y.Y., Dorigo, W., Wagner, W., 2011. Error estimates for near-real-time satellite soil moisture as derived from the land parameter retrieval model. IEEE Geosci. Remote. Sens. Lett. 8 (4), 779–783. http://dx.doi.org/10.1109/LGRS.2011.2114872.

Pellarin, T., Laurent, J.-P., Cappelaere, B., Decharme, B., Descroix, L., Ramier, D., 2009. Hydrological modelling and associated microwave emission of a semi-arid region in South-western Niger. J. Hydrol. 375, 262–272. http://dx.doi.org/10.1016/j.jhydrol.2008.12.003.

Peng, C., Zeng, J., Chen, K.-S., Ma, H., Letu, H., Zhang, X., Shi, P., Bi, H., 2025. Spatial representativeness of soil moisture stations and its influential factors at a global scale. IEEE Trans. Geosci. Remote. Sensing 63, 1–15. http://dx.doi.org/10.1109/TGRS.2024.3523484.

Petropoulos, G.P., McCalmont, J.P., 2017. An operational in situ soil moisture & soil temperature monitoring network for west Wales, UK: The WSMN network. Sensors 17 (7), 1481. http://dx.doi.org/10.3390/s17071481.

Preimesberger, W., Scanlon, T., Su, C.-H., Gruber, A., Dorigo, W., 2021. Homogenization of structural breaks in the global ESA CCI soil moisture multisatellite climate data record. IEEE Trans. Geosci. Remote Sens. 59 (4), 2845–2862. http://dx.doi.org/10.1109/TGRS.2020.3012896.

Raffelli, G., Previati, M., Canone, D., Gisolo, D., Bevilacqua, I., Capello, G., Biddoccu, M., Cavallo, E., Deiana, R., Cassiani, G., Ferraris, S., 2017. Local- and plot-scale measurements of soil moisture: Time and spatially resolved field techniques in plain, hill and mountain sites. Water 9 (9), http://dx.doi.org/10.3390/w9090706, article 706.

Reichle, R.H., Crow, W.T., Keppenne, C.L., 2008. An adaptive ensemble Kalman filter for soil moisture data assimilation. Water Resour. Res. 44 (3), http://dx.doi.org/10.1029/2007WR006357.

Rodell, M., Houser, P.R., Jambor, U., Gottschalck, J., Mitchell, K., Meng, C.-J., Arsenault, K., Cosgrove, B., Radakovich, J., Bosilovich, M., Entin, J.K., Walker, J.P., Lohmann, D., Toll, D., 2004. The global land data assimilation system. Bull. Am. Meteorol. Soc. 85 (3), 381–394. http://dx.doi.org/10.1175/BAMS-85-3-381.

Rosnay, P., Gruhier, C., Timouk, F., Baup, F., Mougin, E., Hiernaux, P., Kergoat, L., Le Dantec, V., 2009. Multi-scale soil moisture measurements at the Gourma meso-scale site in Mali. J. Hydrol. 375, 241–252. http://dx.doi.org/10.1016/j.jhydrol.2009.01.015.

SAF, H., 2021. Algorithm theoretical baseline document (ATBD) metop ASCAT surface soil moisture climate data record v7 12.5 km sampling (H119) and extension (H120). v0.1, EUMETSAT.

Scanlon, T., Pasik, A., Dorigo, W., de Jeu, R.A.M., Hahn, S., van der Schalie, R., Wagner, W., Kidd, R., Gruber, A., 2022. Algorithm theoretical baseline document (ATBD) of ESA CCI soil moisture supporting product version 07.1, V3 issue 1.0, ESA cci.

Schaefer, G., Cosh, M., Jackson, T., 2007. The USDA natural resources conservation service soil climate analysis network (SCAN). J. Atmos. Ocean. Technol. 24 (12), 2073–2077. http://dx.doi.org/10.1175/2007JTECHA930.1.

Scipal, K., Holmes, T., de Jeu, R., Naeimi, V., Wagner, W., 2008. A possible solution for the problem of estimating the error structure of global soil moisture data sets. Geophys. Res. Lett. 35 (24), http://dx.doi.org/10.1029/2008GL035599.

Shuman, D.I., Nayyar, A., Mahajan, A., Goykhman, Y., Li, K., Liu, M., Teneketzis, D., Moghaddam, M., Entekhabi, D., 2010. Measurement scheduling for soil moisture sensing: From physical models to optimal control. Proc. IEEE 98 (11), 1918–1933. http://dx.doi.org/10.1109/JPROC.2010.2052532.

Smith, A., Walker, J., Western, A., Young, R., Ellett, K., Pipunic, R., Grayson, R., Siriwardena, L., Chiew, F., Richter, H., 2012. The Murrumbidgee soil moisture monitoring network data set. Water Resour. Res. 48 (7), http://dx.doi.org/10.1029/2012WR011976.

Stoffelen, A., 1998. Toward the true near-surface wind speed: Error modeling and calibration using triple collocation. J. Geophys. Res.: Ocean. 103 (C4), 7755–7766. http://dx.doi.org/10.1029/97JC03180.

Stradiotti, P., Gruber, A., Preimesberger, W., Dorigo, W., 2025. Study data for accounting for seasonal retrieval errors in the merging of multi-sensor satellite soil moisture products. http://dx.doi.org/10.48436/z0zzp-f4j39.

Su, C.-H., Ryu, D., Crow, W.T., Western, A.W., 2014. Stand-alone error characterisation of microwave satellite soil moisture using a Fourier method. Remote. Sens. Environ. 154, 115–126. http://dx.doi.org/10.1016/j.rse.2014.08.014.

Su, Z., Wen, J., Dente, L., Velde, R.V.D., Wang, L., Ma, Y., Yang, K., Hu, Z., 2011. The Tibetan plateau observatory of plateau scale soil moisture and soil temperature (Tibet-Obs) for quantifying uncertainties in coarse resolution satellite and model products. Hydrol. Earth Syst. Sci. 15 (7), 2303–2316.

Tagesson, T., Fensholt, R., Guiro, I., Rasmussen, M., Huber, S., Mbow, C., Garcia, M., Horion, S., Sandholt, I., Holm-Rasmussen, B., Göttsche, F.-M., Ridler, M., Boke-Olén, N., Olsen, J., Ehammer, A., Madsen, M., Olesen, F., Ardö, J., 2014. Ecosystem properties of semi-arid savanna grassland in West Africa and its relationship to environmental variability. Global Change Biol. 21 (1), 250–264. http://dx.doi.org/10.1111/gcb.12734.

van der Schalie, R., de Jeu, R.A.M., Kerr, Y.H., Wigneron, J.P., Rodríguez-Fernández, N.J., Al-Yaari, A., Parinussa, R.M., Mecklenburg, S., Drusch, M., 2017. The merging of radiative transfer based surface soil moisture data from SMOS and AMSR-E. Remote Sens. Environ. 189, 180–193. http://dx.doi.org/10.1016/j.rse.2016.11.026.

Van der Schalie, R., De Jeu, R., Parinussa, R., Rodríguez-Fernández, N., Kerr, Y., Al-Yaari, A., Wigneron, J.-P., Drusch, M., 2018. The effect of three different data fusion approaches on the quality of soil moisture retrievals from multiple passive microwave sensors. Remote. Sens. 10 (1), http://dx.doi.org/10.3390/rs10010107, article 107.

van der Vliet, M., van der Schalie, R., Rodriguez-Fernandez, N., Colliander, A., de Jeu, R., Preimesberger, W., Scanlon, T., Dorigo, W., 2020. Reconciling flagging strategies for multi-sensor satellite soil moisture climate data records. Remote. Sens. 12 (20), http://dx.doi.org/10.3390/rs12203439, article 3439.

Vreugdenhil, M., Dorigo, W., Broer, M., Haas, P., Eder, A., Hogan, P., Blöschl, G., Wagner, W., 2013. Towards a high-density soil moisture network for the validation of SMAP in Petzenkirchen, Austria. In: 2013 IEEE International Geoscience and Remote Sensing Symposium - IGARSS. IEEE, pp. 1865–1868. http://dx.doi.org/10.1109/IGARSS.2013.6723166.

Vreugdenhil, M., Dorigo, W.A., Wagner, W., de Jeu, R.A.M., Hahn, S., van Marle, M.J.E., 2016. Analyzing the vegetation parameterization in the TU-Wien ASCAT soil moisture retrieval. IEEE Trans. Geosci. Remote Sens. 54 (6), 3513–3531. http://dx.doi.org/10.1109/TGRS.2016.2519842.

Vreugdenhil, M., Greimeister-Pfeil, I., Preimesberger, W., Camici, S., Dorigo, W., Enenkel, M., van der Schalie, R., Steele-Dunne, S., Wagner, W., 2022. Microwave remote sensing for agricultural drought monitoring: Recent developments and challenges. Front. Water 4, http://dx.doi.org/10.3389/frwa.2022.1045451.

Wagner, W., Hahn, S., Kidd, R., Melzer, T., Bartalis, Z., Hasenauer, S., Figa, J., De Rosnay, P., Jann, A., Schneider, S., 2013. The ASCAT soil moisture product: A review of its specifications, validation results, and emerging applications. Meteorol. Z. 22 (1), 1–29.

Wagner, W., Lemoine, G., Rott, H., 1999. A method for estimating soil moisture from ERS scatterometer and soil data. Remote Sens. Environ. 70 (2), 191–207. http://dx.doi.org/10.1016/S0034-4257(99)00036-X.

Wagner, W., Lindorfer, R., Hahn, S., Kim, H., Vreugdenhil, M., Gruber, A., Fischer, M., Trnka, M., 2024. Global scale mapping of subsurface scattering signals impacting ASCAT soil moisture retrievals. IEEE Trans. Geosci. Remote Sens..

Wigneron, J.-P., Dayan, S., Kruszewski, A., Aluome, C., Al-Yaari, A., Fan, L., Guven, S., Chipeaux, C., Moisy, C., Guyon, D., Loustau, D., 2018. The aqui network: Soil moisture sites in the les landes forest and graves vineyards (Bordeaux Aquitaine Region, France). In: IGARSS 2018-2018 IEEE International Geoscience and Remote Sensing Symposium. IEEE, pp. 3739–3742. http://dx.doi.org/10.1109/IGARSS.2018.8517392.

Wu, K., Ryu, D., Nie, L., Shu, H., 2021. Time-variant error characterization of SMAP and ASCAT soil moisture using triple collocation analysis. Remote Sens. Environ. 256, 112324. http://dx.doi.org/10.1016/j.rse.2021.112324.

Xaver, A., Zappa, L., Rab, G., Pfeil, I., Vreugdenhil, M., Hemment, D., Dorigo, W.A., 2020. Evaluating the suitability of the consumer low-cost parrot flower power soil moisture sensor for scientific environmental applications. Geosci. Instrum. Methods Data Syst. 9 (1), 117–139. http://dx.doi.org/10.5194/gi-9-117-2020.

Yang, K., Qin, J., Zhao, L., Chen, Y., Tang, W., Han, M., Zhu, L., Chen, Z., Lv, N., Ding, B., Wu, H., Lin, C., 2013. A multi-scale soil moisture and freeze-thaw monitoring network on the third pole. Bull. Am. Meteorol. Soc. 94, 1907–1916. http://dx.doi.org/10.1175/BAMS-D-12-00203.1.

Young, R., Walker, J., Yeoh, N., Smith, A., Ellett, K., Merlin, O., Western, A., 2008. Soil Moisture and Meteorological Observations from the Murrumbidgee Catchment. Department of Civil and Environmental Engineering, The University of Melbourne.

Zacharias, S., Bogena, H., Samaniego, L., Mauder, M., Fuß, R., Pütz, T., Frenzel, M., Schwank, M., Baessler, C., Butterbach-Bahl, K., Bens, O., Borg, E., Brauer, A., Dietrich, P., Hajnsek, I., Helle, G., Kiese, R., Kunstmann, H., Klotz, S., Vereecken, H., 2011. A network of terrestrial environmental observatories in Germany. Vadose Zone J. 10, 955–973. http://dx.doi.org/10.2136/vzj2010.0139.

Zappa, L., Forkel, M., Xaver, A., Dorigo, W., 2019. Deriving field scale soil moisture from satellite observations and ground measurements in a Hilly Agricultural Region. Remote. Sens. 11 (22), http://dx.doi.org/10.3390/rs11222596, article 2596.

Zappa, L., Woods, M., Hemment, D., Xaver, A., Dorigo, W., 2020. Evaluation of remotely sensed soil moisture products using crowdsourced measurements. In: Eighth International Conference on Remote Sensing and Geoinformation of Environment. SPIE, Cyprus.

Zhao, T., Shi, J., Lv, L., Xu, H., Chen, D., Cui, Q., Jackson, T.J., Yan, G., Jia, L., Chen, L., et al., 2020. Soil moisture experiment in the Luan river supporting new satellite mission opportunities. Remote Sens. Environ. 240, 111680. http://dx.doi.org/10.1016/j.rse.2019.111680.

Zheng, J., Zhao, T., Lü, H., Shi, J., Cosh, M.H., Ji, D., Jiang, L., Cui, Q., Lu, H., Yang, K., et al., 2022. Assessment of 24 soil moisture datasets using a new in situ network in the Shandian river basin of China. Remote Sens. Environ. 271, 112891. http://dx.doi.org/10.1016/j.rse.2021.112891.

Zreda, M., Desilets, D., Ferré, T., Scott, R., 2008. Measuring soil moisture content non-invasively at intermediate spatial scale using cosmic-ray neutrons. Geophys. Res. Lett. 35 (21), http://dx.doi.org/10.1029/2008GL035655.

Zreda, M., Shuttleworth, W.J., Zeng, X., Zweck, C., Desilets, D., Franz, T., Rosolem, R., 2012. COSMOS: The cosmic-ray soil moisture observing system. Hydrol. Earth Syst. Sci. 16 (11), 4079–4099. http://dx.doi.org/10.5194/hess-16-4079-2012.

Zwieback, Z., Colliander, A., Cosh, M.H., Martínez-Fernández, J., McNairn, H., Starks, P.J., Thibeault, M., Berg, A., 2018. Estimating time-dependent vegetation biases in the SMAP soil moisture product. Hydrol. Earth Syst. Sci. 22, 4473–4489. http://dx.doi.org/10.5194/hess-22-4473-2018.

Zwieback, S., Dorigo, W., Wagner, W., 2012a. Temporal error variability of coarse scale soil moisture products - case study in central Spain. In: 2012 IEEE International Geoscience and Remote Sensing Symposium. pp. 722–725. http://dx.doi.org/10.1109/IGARSS.2012.6351463.

Zwieback, S., Scipal, K., Dorigo, W., Wagner, W., 2012b. Structural and statistical properties of the collocation technique for error characterization. Nonlinear Process. Geophys. 19 (1), 69–80. http://dx.doi.org/10.5194/npg-19-69-2012.